HIGH FREQUENCY PLASMA GENERATORS FOR ION THRUSTERS

PREPARED FOR

LEWIS RESEARCH CENTER

NATIONAL AERONAUTICS AND SPACE ADMINISTRATION

CONTRACT NO. NAS3-22473

BY

HEINZ GOEDE

WILLIAM F. DIVERGILIO

VERRYL L. FOSNIGHT

GENE K. KOMATSU

FINAL REPORT

JULY 1984

TRW

1. Report No. NASA CR 174772	2. Government Accession No.	3. Recipient's Catalog No.
4. Title and Subtitle High Frequency Plasma Generator for ION Thrusters		5. Report Date July 1984 6. Performing Organization Code
7. Author(s) Heinz Goede, William F. Di Vergilio, Verryl V. Fosnight, G. Komatsu		8. Performing Organization Report No. 10. Work Unit No.
9. Performing Organization Name and Address TRW One Space Park Redondo Beach, CA 90278		11. Contract or Grant No. NAS3-22473 13. Type of Report and Period Covered Final, 9/80-4/83
12. Sponsoring Agency Name and Address NASA Lewis Research Center 2100 Brookpark Rd. Cleveland, OH 44135		14. Sponsoring Agency Code

15. Supplementary Notes

NASA Contract Monitor
Shigeo Nakanishi
NASA Lewis Research Center

TRW Program Manager
Gene Komatsu
One Space Park, Redondo Beach, CA

16. Abstract The results of a program to experimentally develop two new types of plasma generators for 30.cm electrostatic. Argon ion thrusters are presented. The two plasma generating methods selected for this study were by radio frequency induction (RFI), operating at an input power frequency of 1.MHz, and by electron cyclotron heating (ECH) at an operating frequency of 5.0 GHz. Both of these generators utilize multi-line cusp permanent magnet configurations for plasma confinement and beam profile optimization. The program goals were to develop a plasma generator possessing the characteristics of high electrical efficiency (low eV/ion) and simplicity of operation while maintaining the reliability and durability of the conventional hollow-cathode plasma sources. The RFI plasma generator has achieved minimum discharge losses of 120.eV/ion while the ECH generator has obtained 145.eV/ion, assuming a 90% ion optical transparency of the electrostatic acceleration system. Details of experimental tests with a variety of magnet configurations are presented in this report.

17. Key Words (Suggested by Author(s))
Electrostatic Thruster
Radio Frequency Induction
Electron Cyclotron Heating
Multi-cusp, Plasma sources

18. Distribution Statement
Unclassified - Unlimited

19. Security Classif. (of this report)	20. Security Classif. (of this page)	21. No. of Pages	22. Price*
Unclassified	Unclassified		

*For sale by the Clearinghouse for Federal Scientific and Technical Information
Springfield, Virginia 22151

CONTENTS

1. PROGRAM SUMMARY

This report represents the results of an experimental program to adapt two types of high frequency plasma generators for low thrust, 30 cm, electrostatic argon ion thrusters. The initial scope of this "High Frequency Plasma Generator" program placed no direct constraints on the method of coupling power to the plasma or on the choice of magnetic field configuration used to enhance the plasma production efficiency. Aside from providing a back-up concept to the more mature, conventional hollow-cathode-based plasma sources, a goal in the present program was to develop a plasma generator which has a high electrical efficiency, a parameter which is of importance for low specific impulse engines.

The two methods selected for coupling electrical power to the plasma generator were (1) Radio Frequency Induction (RFI) which operates in the frequency range of several hundred kilohertz to several megahertz and (2) by Electron Cyclotron Heating (ECH) which operates in the range of several gigahertz. The RFI generator, like the hollow-cathode plasma source, does not fundamentally require the presence of magnetic fields for its operation but the ECH generator by its principle of operation does require that rather strong magnet fields be present inside the engine housing.

The class of magnetic field geometry which was used for both types of high frequency generators is variously known as a "multicusp," "multipole," or "multidipole" configuration and is particularly well suited to thruster applications since permanent magnets are used. Permanent magnets, while adding mass to the thruster, use no electrical power to provide strong particle confinement fields and can be arranged into geometries which produce very low magnetic field strengths both in the central volume of the plasma general and at the ion extraction plane. Low fields at these locations are thought to be an aid in the production of a more uniform beam profile and are also required for the ion extraction system (which is a field-free ion optics design) and the beam neutralization process.

During the initial phase of this program much of the work on the RFI source consisted of experimentation and modeling of the power coupling between the RF section and the plasma. Some experimentation was carried out to measure the electron and ion confinement which has a direct impact on

the beam production efficiency. One magnetic confinement geometry, namely an axial line cusp, was studied. The results indicate that considerable cross field argon ion transport to the walls occurs and that reduction of this transport is the major mechanism by which the eV/ion value can be improved. It was demonstrated that doubling the permanent magnet pole face field strength by replacing ceramic magnets (1.5K gauss) with samarium cobalt magnets (3.0K gauss) in the same configuration produced negligible (<5.%) change in the eV/ion. Ceramic magnets which can operate at higher temperatures may therefore be preferred over the more costly rare-earth magnets. This RFI thruster was tested at NASA-Lewis Research Center; it produced a continuous 1 KeV, 3.0 ampere Argon ion beam with minimum discharge losses of 220 ±10 eV/ion at a propellant utilization of 45 percent. The details of the development of the RFI plasma source under the first half of the program can be found in the Interim Report, NASA CR-167957.

The second half of the program which is described in this report emphasized, in the development of the RFI plasma generator, work toward the reduction in the eV/ion and toward the production of a flatter beam profile. Several plasma generators were built and tested with a variety of permanent magnet configurations. The axial line cusp geometry was replaced by a ring-cusp geometry in which the permanent magnets formed azimuthal rings about the cylindrical shell of the thruster. This geometry had the flexibility for testing various magnet sizes and their spacing; in addition, it allowed for a natural termination by soft iron of the magnetic field lines closest to the extraction plane which gave considerable improvement in the "beam" profile. The best results obtained was an eV/ion of 120 (assuming 90 percent transparency optics) with a "beam" flatness parameter of >90 percent for a 30 cm diameter extraction grid. As no actual beam extraction was performed with this improved RFI generator, no propellant utilization data is available at the time this report was written.

The discharge characteristics and electrical efficiency of the ECH plasma generator were also experimently examined in several different cusp magnetic confinement geometries during the first half of this program. In these experiments plasma was produced with microwave power at a frequency of 5 GHz. The electron heating process required magnetic field strengths of at least 1.8 K gauss in the interior of the plasma generator and, as a

consequence, required the use of rare-earth permanent magnets in all of the experiments. Discharges with axial as well as azimuthal line cusp geometries were characterized; the latter geometry provided the best result of 145 eV/ion (again assuming a 90 percent ion transparency extraction system). Beam extraction for these experiments was simulated by replacing the two grid acceleration optics with a biased termination plate.

During the second half of the program the ECH plasma generator concept was tested with a quite different magnetic geometry; a divergent volume magnetic field was produced by small, 15 cm diameter, pancake electromagnets. The plasma produced by electron cyclotron heating was confined radially by the nearly solenoidal volume magnetic field and axially by electrostatic reflection and adiabatic action of the particles. The purpose of these experiments was not so much to develop a new thruster configuration but rather to examine cross field plasma transport. The knowledge gained from these experiments would hopefully aid in the development of both the RFI and ECH multi-cusp geometry concepts already mentioned above. However, experiments with plasma production in the solenoidal B-field geometry indicated that particle losses axially dominated considerably over radial transport; in fact, discharge start-up proved to be difficult at the usual operating neutral pressures. In addition several perplexing results, which are described in this report, were obtained with these experiments. An important result shown by all ECH experiments conducted under this program is that the maximum ion beam current that can be extracted from the generator is limited not by the available microwave power, but by the plasma cutoff density condition $\omega_{pe} = \omega_{\mu}$, where ω_{pe} is the plasma frequency and ω_{μ} is the radian frequency of the applied power.

2. PROGRAM INTRODUCTION

Mercury has until recently been the propellant used in the development of thrusters for primary electric propulsion. Indeed, the 30 cm mercury thruster is the only technology-ready thruster available. However, due to low spacecraft contamination and environmental advantages over mercury, primary propulsion thrusters using inert gases as propellant have been receiving great interest. Of the inert gases the most cost effective propellant is argon and consequently it is receiving the most attention in current research and development.

Studies have shown that the attainment of increased efficiencies for ion thrusters at low (1000 to 2000 seconds) specific impulse would greatly decrease the overall cost of many proposed geocentric missions which would utilize electric propulsion. The requirement of low specific impulse places more of the emphasis on the electrical efficiency of the plasma generator and its associated power conditioners for attaining high system electrical efficiency. The specific impulse is

$$I_{sp} = \frac{1}{g_o} \left(\frac{2qV}{m}\right)^{1/2}$$

where g_o is the acceleration due to gravity at the earth's surface, V is the net accelerating potential, and q/m is the ion charge to mass ratio. To maintain a high thrust at low I_{sp} requires lowering V and increasing the beam current. For argon with a high q/m (compared to mercury), V must be lowered further. On the other hand, the thruster system power is equal to the product of V and the beam current plus losses that to first order go as the beam current. Hence, the losses that are roughly proportional to beam current must be lowered to take maximum advantage of a lower specific impulse.

The importance of increasing the plasma generator efficiency in order to increase the total system efficiency can also be seen from the following. For electrostatic thrusters the largest share of electrical power supplied by the system power processor goes to form the thrust producing energetic ion beam. State-of-the-art electrostatic acceleration systems (that is, physical multi-hole grid structures) produce this beam very efficiently;

efficiencies of better than 99 percent (not including power conditioning losses) are not uncommon. The next largest portion of thruster system power is that used to generate the plasma inside the ion chamber. Clearly, the system efficiency will be increased if these plasma ions can be extracted to form the beam before being lost by recombination either in the chamber volume or at the walls. It should be noted, however, that large increases in the plasma production and confinement efficiency may not necessarily have a large impact on the overall system efficiency. For example, let us say that it takes 800 watts to produce a plasma from which a 4 Amp, 1K volt beam can be extracted. The total energy efficiency (excluding power conditioning losses) would be 4000/4800 = 83 percent. Now, if through some means, the plasma production costs could be reduced by a factor of two so that only 400 watts are required to produce a plasma from which a 4 Amp, 1K volt beam can be extracted, then the system efficiency increases by only 8 percent, even though the production costs have been reduced by 50 percent.

The main goal of the present program was to develop two new plasma generator concepts which showed promise of reducing the energy expenditure for plasma production. Recently, tests with high frequency plasma devices have indicated that plasmas of a few cubic meters volume of various gases can be obtained at ion production costs approaching 50 eV/ion. If such costs could be obtained with ion thrusters, increases in system efficiency of 30 percent or greater could be obtained at low (1400 seconds) specific impulse.

The two argon plasma generating methods selected for experimental study were a radio frequency induction (RFI) source and an electron cyclotron heated (ECH) plasma source operating at microwave frequencies.

The RFI source described in Section 3 is a new approach for production of dense plasmas that was developed at TRW. It offers a number of advantages over hot cathode dc charges. The major advantage is a very large reduction in the average electron current lost from the plasma to electron absorbing elements, because the dc cathode-anode arrangement is replaced by an internal rf antenna. Other advantages include simplicity of operation and control, potentially higher durability, and a startup time of the few seconds. It uses conventional extraction optics and multicusp magnetic geometry for plasma confinement.

The ECH or microwave source described in Section 4 also uses conventional electrostatic optics and multicusp confinement but is otherwise electrodeless. The plasma is produced by applying microwaves at a frequency equal to the cyclotron frequency of electrons in the confining magnetic field inside the thruster chamber. It offers all of the advantages of the rf source plus very higher durability since it has no electrodes.

The class of magnetic field geometry used for each concept is variously known as "multicusp," "multipole," or "multidipole," and is particularly well suited to thruster applications as it may utilize permanent magnets which require no additional power and provide fields strong enough to confine ions. Additionally, multicusp geometries with very low magnetic fields in the extraction region are possible. Such geometries were first used at Electro Optical Systems[1] for thruster applications, and later adapted with a somewhat different electrical configuration, for laboratory plasma sources[2] and neutral beam applications[3].

The results of efforts under the first half of this program are described in Reference 4. The remainder of this report represents the efforts of the second half of the program for the development of high frequency plasma generators for 30 cm Argon thruster applications.

3. RFI THRUSTER DEVELOPMENT

3.1 INTRODUCTION

RF induction plasmas generated with a coil antenna surrounding a quartz vessel were first described by Hittorf[1], and have since been used for studies of basic discharge physics[2,3], in electrostatic thruster applications[4], and as light sources for spectroscopic studies.

Adaptation of the rf induction technique to multicusp geometries was first made at TRW in connection with the development of laboratory plasma sources. Simply, a dielectric coated coil antenna is situated in the weak magnetic field region of a multicusp device and resonated at the desired frequency with external capacitors and inductors. Electrons are collisionally heated in the electric fields induced in the plasma by the circulating coil current. Since the electron heating takes place in the weak magnetic field region, the confinement properties of the system are very similar to those of a dc discharge (i.e., filament or hollow cathode discharge) in a multicusp geometry. In all applications of this technique to date the entire (conducting) wall of the containment vessel, with the exception of the optics, is one common "electrode," with respect to which the plasma assumes a positive potential. The plasma is cusp confined[5] at the magnet pole faces and transport to the walls between magnets is inhibited by the strong magnetic fields.

A complete model of heating in the RFI Multicusp source has not yet been developed, but the basic physics is well described by simple fluid theory. The electron equation of motion in the induced electric field is

$$\frac{d\vec{v}}{dt} = -\frac{e}{m}\vec{E} - \upsilon\vec{v} \tag{3.1}$$

Where υ is th total electron momentum transfer collision frequency. Taking $\vec{E}$ and $\vec{v}$ as complex with time dependence $e^{-i\omega t}$, the solution of (3.1) is

$$\vec{v} = \frac{-e\vec{E}}{m(\upsilon - i\omega)} \tag{3.2}$$

We may express the plasma response in terms of Ohm's law

$$\vec{j} = - n_e e \vec{v} = \sigma \vec{E} \tag{3.3}$$

with complex conductivity

$$\sigma = \sigma_R + i\sigma_I = \frac{\upsilon + i\omega}{\upsilon^2 + \omega^2} \frac{n_e e^2}{m} \tag{3.4}$$

It may be seen from (3.4) that the plasma response consists of a resistive part and a reactive part.

The power coupled to the plasma is given by the volume integral

$$P = \int \vec{j} \cdot \vec{E}\, dV = \frac{1}{2} \int \sigma_R |E|^2\, dV \tag{3.5}$$

or

$$P = \frac{1}{2} \int \frac{n_e e^2}{m} \frac{\upsilon}{\upsilon^2 + \omega^2} |E| \quad dV^2 \tag{3.6}$$

With the assumption that n_e and υ are spatially uniform in the heating region, this may be written for time-averaged power as,

$$P = \frac{n_e e^2}{m} \frac{\upsilon}{\upsilon^2 + \omega^2} \langle E^2 V \rangle \tag{3.7}$$

where

$$\langle E^2 V \rangle \equiv \frac{1}{2} \int |E|^2\, dV \tag{3.8}$$

In order to sustain a discharge through rf heating, the input power given by (3.7) must balance the discharge power, P_D, given by

$$P_D = n_e n_o (\langle \sigma v_e \rangle_i \varepsilon_i + \langle \sigma v_e \rangle_{ex} \varepsilon_{ex}) V_{pp} + \frac{1}{2} n_e c_s A (2kT_e + e\phi_p) \tag{3.9}$$

where ε_i and ε_{ex} are the ionization energy and average excitation energy and $\langle \sigma v \rangle_i$ and $\langle \sigma v_e \rangle_{ex}$ are averages over the electron distribution function of the ionization and excitation cross sections respectively. The electron density and temperature is assumed uniform in the plasma production volume V_{pp}, and the particle loss rate is expressed as the Bohm current over an effective area, A. Expression (3.9) may be written

$$P_D = n_e p_d \tag{3.10}$$

where p_d is the discharge power per unit electron density, and is independent of electron density. Equating (3.7) and (3.10) gives the breakdown requirement

$$\langle E^2 \nu \rangle = \frac{m}{e^2} \frac{\nu^2 + \omega^2}{\nu} p_d \tag{3.11}$$

which is independent of density if ν is density independent. If the spatial structure of the electric field is independent of density and frequency, which will be the case for sufficiently low density, then

$$|E|^2 \propto \frac{\nu^2 + \omega^2}{\nu} \tag{3.12}$$

which is familiar as the form of the Paschen high frequency breakdown curve.[5] We may express (3.12) in terms of the antenna current as

$$I_A \propto \frac{|E|}{\omega} \propto \left(1 + \frac{\nu^2}{\omega^2}\right)^{1/2} \nu^{-1/2} \tag{3.13}$$

which result will be referred to in Section 3.3.1.

Returning to equation (3.7), it may be seen that if the electric field structure is independent of density, the input power is directly proportional to the electron density. Then, if the plasma loading of the antenna is modeled as an equivalent parallel resistance, that resistance varies inversely with the electron density. More realistically, it is expected that the electric field will be modified by the plasma skin effect. While the rf antennae used in the thruster are mechanically simple, their electric field patterns are not easily modeled analytically. For the purposes of comparison to the case of fields unmodified by the plasma, corresponding to a skin depth much larger than the antenna radius, we consider the case of the skin depth smaller than the inter-turn spacing of the antenna. The fields may then be approximated as those of an infinite straight rod antenna, which case has been treated by one of the authors[6]. From Reference 6, the main component of the induced field is along the antenna and is given by

$$E = \frac{2i\omega I_A}{c} K_o (\gamma r) \tag{3.14}$$

where K_o is the modified Bessel function[7], c is the speed of light, r is measured from the antenna axis and

$$\gamma = \frac{1}{c} (4\pi i \sigma)^{1/2} \tag{3.15}$$

with σ given by (3.4). We have numerically evaluated the volume integral (3.8) using expression (3.14) with υ/ω as a parameter, and find that, to a good approximation

$$\langle E^2 V \rangle = \frac{4\pi}{c^2} \omega^2 I_A^2 \delta^2 L \tag{3.16}$$

where L is the antenna length, ω_p the plasma frequency and δ is the skin depth,

$$\delta = (1 + \frac{\upsilon^2}{\omega^2})^{1/2} \frac{c}{\omega_p} . \tag{3.17}$$

Expression (3.16) is a good approximation for υ/ω varying from much less than one to much greater than one, as long as the radius of the antenna rod is less than about $\delta/5$. From (3.16), it is apparent that $\langle E^2 V \rangle$ is inversely proportional to density in this extreme case, and therefore, from (3.7), the input power is independent of density. If the plasma is modeled as a parallel resistance to the antenna, the resistance is independent of density.

3.2 APPARATUS

3.2.1 Thruster Assembly

The basic RFI thruster assembly is shown in Figure 3-1. It consisted of a 33 cm diameter, 20 cm long, cylindrical shell made from 1 mm 304 stainless steel welded to front and back mounting rings. SHAG (small hole accel grid) screen and accelerator electrodes were mounted on the exhaust and insulated from the main housing with thin sheets of reconstituted mica; the screen and accelerator could thus be biased separately with respect to the shell. The other end of the cylinder was formed from 1 mm stainless steel sheet. The first experimental RFI thruster utilized a magnetic geometry known as an axial line cusp with 12 bar magnets of alternating magnetic

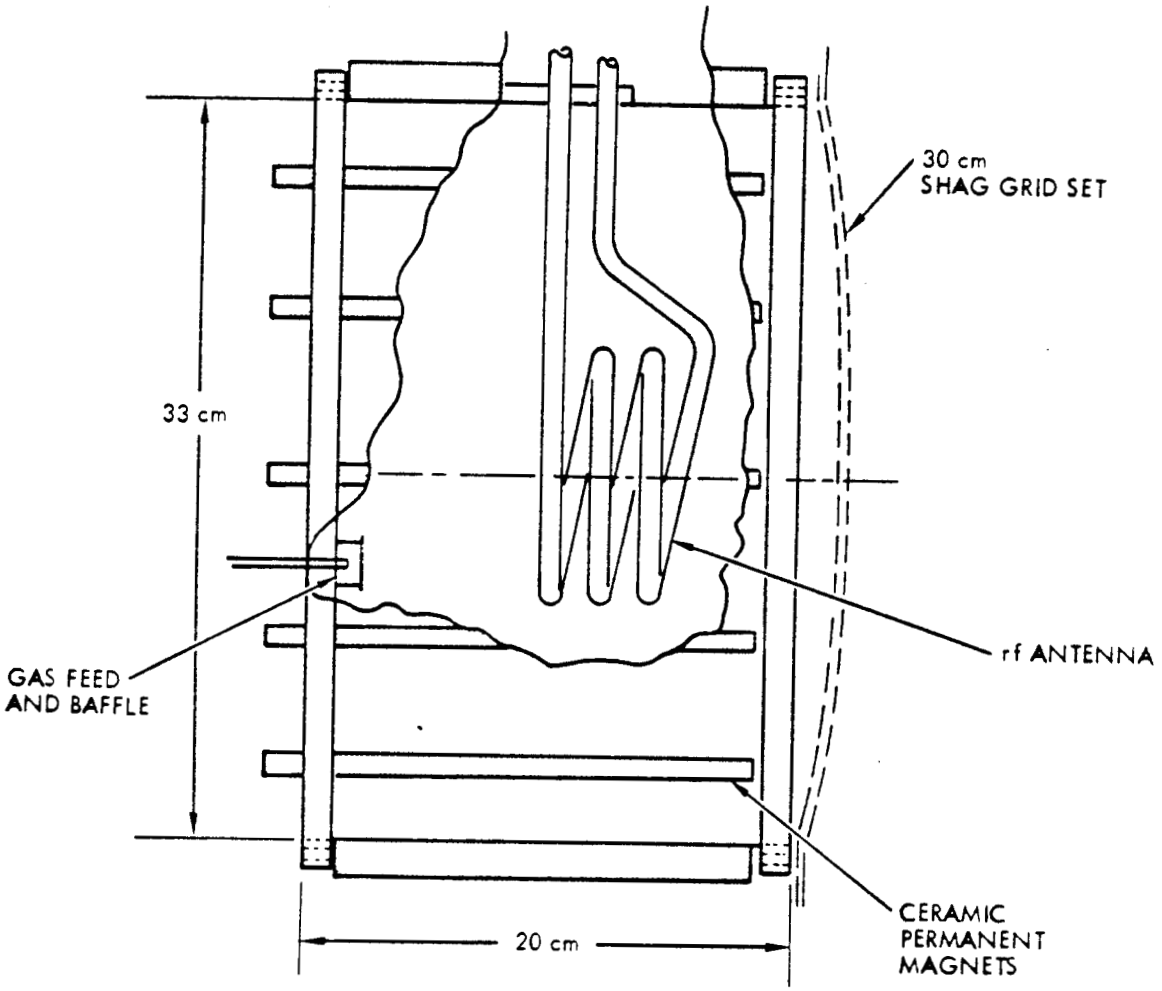

Figure 3.1 Schematic of the RFI Thruster

Figure 3-1. Schematic of the RFI Thruster

polarity and uniform spacing mounted around the cylindrical shell. Five bar magnets continued the line cusps across the backplate. The type of magnets chosen were ceramic, with dimensions 1.9 cm wide by 2.5 cm in the direction of magnetization. These magnets have a measured pole face field strength of 1.5 KG. A 2.5 mm thick soft iron plate-pole piece completed the magnetic circuit external to the shell for the five backplate magnets. Argon propellant was fed into the thruster through the backplate near the axis. The argon feed line contained a nonconducting section for high voltage isolation of the laboratory gas supply located outside the vacuum chamber. Various copper antennas were suspended axially from a block of insulating material mounted on the outside of the thruster shell. Each antenna was sheathed with a 1 mm thick dielectric to prevent direct ion impingment and thus protect the antenna from sputtering.

To initiate the discharge a 5 cm long, 0.007-inch diameter Tungsten filament was positioned inside the thruster about 5 cm from the wall. This filament was biased 40 volts negative with respect to the thruster shell and heated to a temperature such that approximately 10 mA of emission current was drawn. Once the discharge was ignited the filament power could be shut off and the discharge could be maintained by the RF power alone.

3.2.2 RF Power System

Various power amplifier configurations and matching network configurations were utilized throughout the program depending upon the desired operating frequency and power level. For studies of the frequency dependence of rf discharge characteristics, two broadband Class A amplifiers (ENI A-300) were operated in a push-pull fashion with a combined total power of 600 watts maximum available to drive the antenna resonant circuit. For beam extraction tests performed at the NASA/Lewis Research Center Test Facility, a Class C amplifier operating at 1.5 MHz with output power in excess of one kilowatt was constructed.

The general power system configuration for all tests, together with the rf diagnostics, is shown in Figure 3-2. The matching network capacitors and inductors were chosen to resonate the antenna at the desired frequency, which during the course of the program varied between 0.35 and 1.75 MHz. The purpose of the ferrite core transformer is to isolate the amplifier system from the matching network; it also aids in impedance

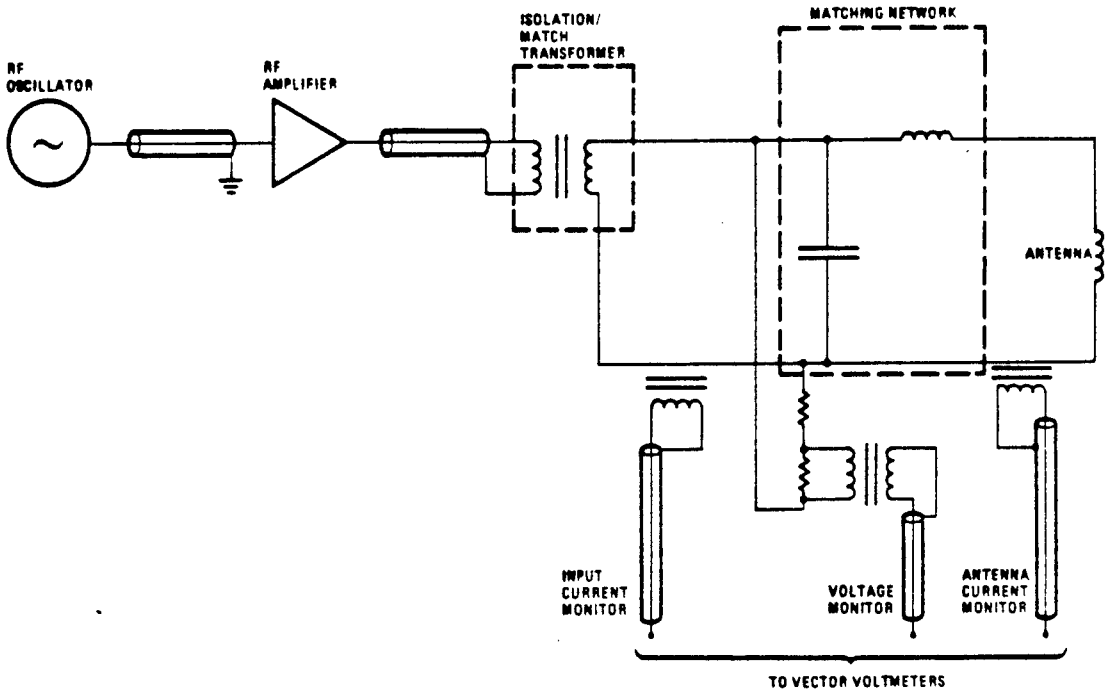

Figure 3-2. RF Power Transmission and Measurement Circuits

matching. The rf input current and antenna current were detected with current transformers. The rf voltage was obtained through an isolated resistive divider. The rms values and relative phase angles of the voltage and currents were measured with vector voltmeters. The vector product of the rf input current and tank voltage ($|I|*|V|* \cos\theta$) is used to calculate the rf input power.

3.2.3 Support Systems

For rf discharge characterization tests at TRW, the thruster was mounted inside a 1.2 meter diameter by 2.1 meter long vacuum chamber pumped by a single 40 cm oil diffusion pump. RF power and start-up filament power were supplied to the thruster through insulated vacuum feedthroughs.

A movable Langmuir probe was inserted through the sidewall of the thruster for measurements of the plasma density and electron temperature profiles.

All thruster characterization at TRW was performed without ion beam extraction. In order to obtain a measurement of the total ion current available at the extraction plane, the screen and accel grids were electrically connected together and biased at a potential of 40 volts negative with respect to the thruster walls. The ion current collected by the combined screen and accel grids, when corrected for the ion transparency of the grids, provided us an approximate value for the equivalent ion beam current that would be expected during actual beam extraction.

Thruster and grid biasing for the ion beam extraction tests performed at NASA/Lewis ReC is shown schematically in Figure 3-3, and is not significantly different than that used for hollow cathode thrusters.

3.3 AXIAL CUSP CONFIGURATION TEST RESULTS

3.3.1 Frequency Dependence of Discharge Efficiency

Discharge efficiency and rf circuit losses were measured at five different frequencies over the range 0.35 to 1.75 MHz. The following procedure was used to separate actual discharge losses, that is, power absorbed by the plasma, from circuit losses. First, the discharge was operated at the desired set of conditions (frequency, gas pressure, and density) and the rf input power and antenna current were recorded. The

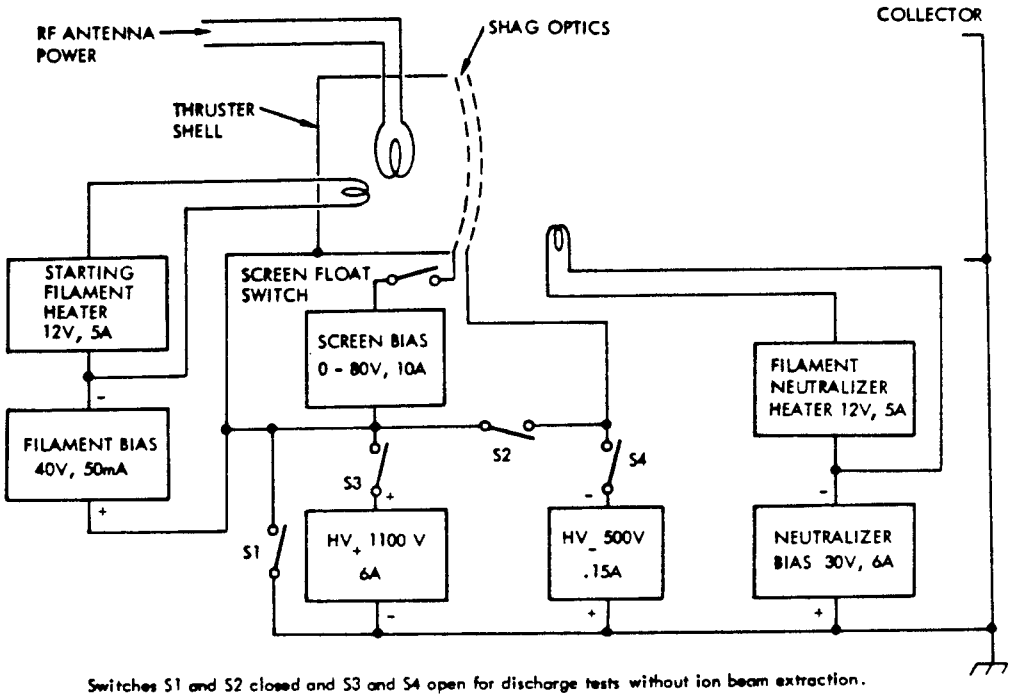

Figure 3-3. Electrical Block Diagram for RF Thruster Tests

propellant gas was then shut off thus extinguishing the discharge and the rf input power at the same antenna current was recorded. This second value of rf input power represents the rf circuit losses while the difference between the two values represents the net discharge power. An example of the application of this technique is given in Figure 3-4. The net discharge power divided by the ion current collected by the biased screen and accel grids gives an approximate value for the discharge losses (eV/ion) uncorrected for screen transparency and does not include rf circuit losses. The discharge losses obtained in this manner are shown as a function of frequency in Figure 3-5. The larger error bars at the low frequencies are due to errors introduced by two factors: 1) a less accurate rf measurement system was used at these frequencies and 2) circuit losses were high, resulting in component heating and lack of stability. We note the significant result that the net discharge losses were independent of the operating frequency within experimental error. One is therefore at liberty to choose the operating frequency on the basis of other considerations such as, for example, the minimizing of rf circuit losses which we now consider.

The two main areas for circuit losses are the conversion losses of the rf oscillator (or power amplifier) and resistive losses in the antenna both of which depend upon the antenna current and frequency. It can be shown that for an rf discharge maintained by electron heating at an effective collision frequency, ν, the antenna current has the frequency dependence given by

$$I_A \propto (1 + \nu^2/\omega^2)^{1/2} \qquad (3.1)$$

under the assumption that the spatial dependence of the induced electric field is not frequency dependent. The measured frequency dependence of the antenna current is illustrated in Figure 3-6. Shown are data points of the product of antenna current and frequency plotted against frequency. Also shown in Figure 3-6 are plots of $I_A f$ with I_A given by equation (3.1) for assumed collision frequencies of 1.0×10^7, 1.5×10^7 and 3×10^7 per second. The theoretical curves are normalized to $I_A f = 21.5$ amp-MHz at $f = 0$ in order to obtain the best fit to the data at the low frequency end.

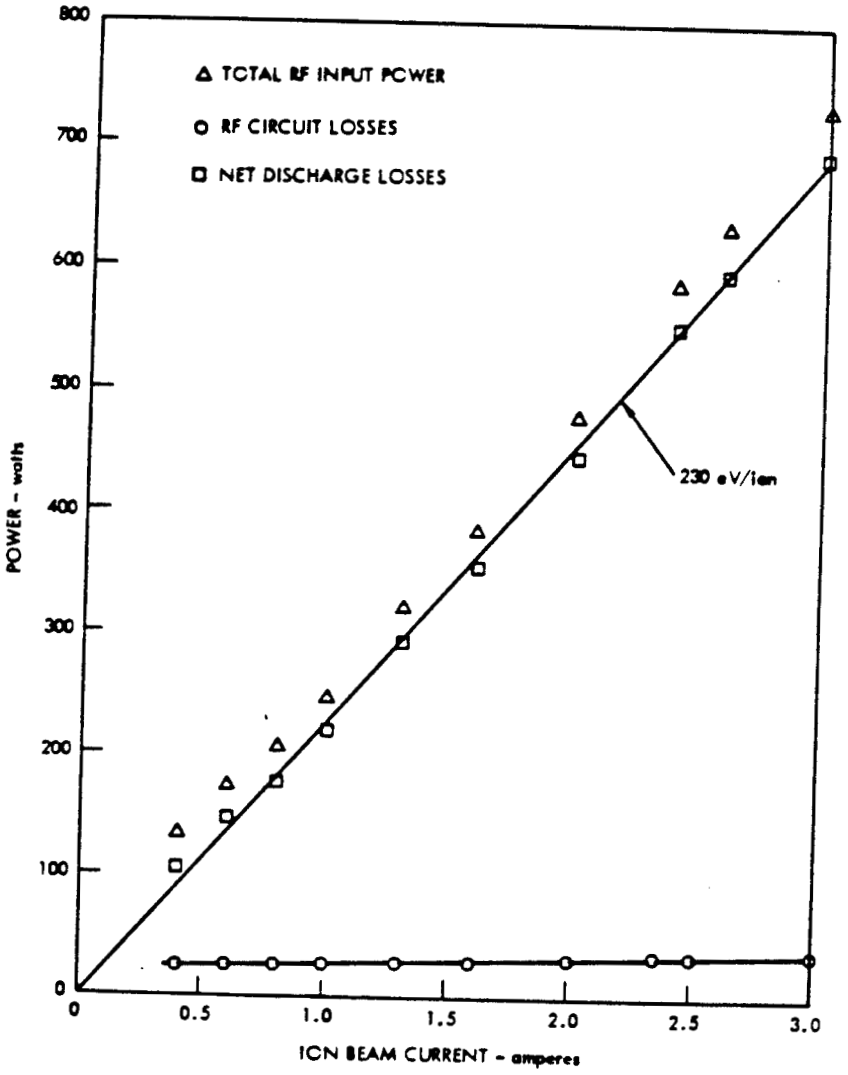

Figure 3-4. Total rf input power, circuit losses, and their difference (net discharge losses) as a function of ion beam current. Argon flow rate was 6.6 ampere equivalent.

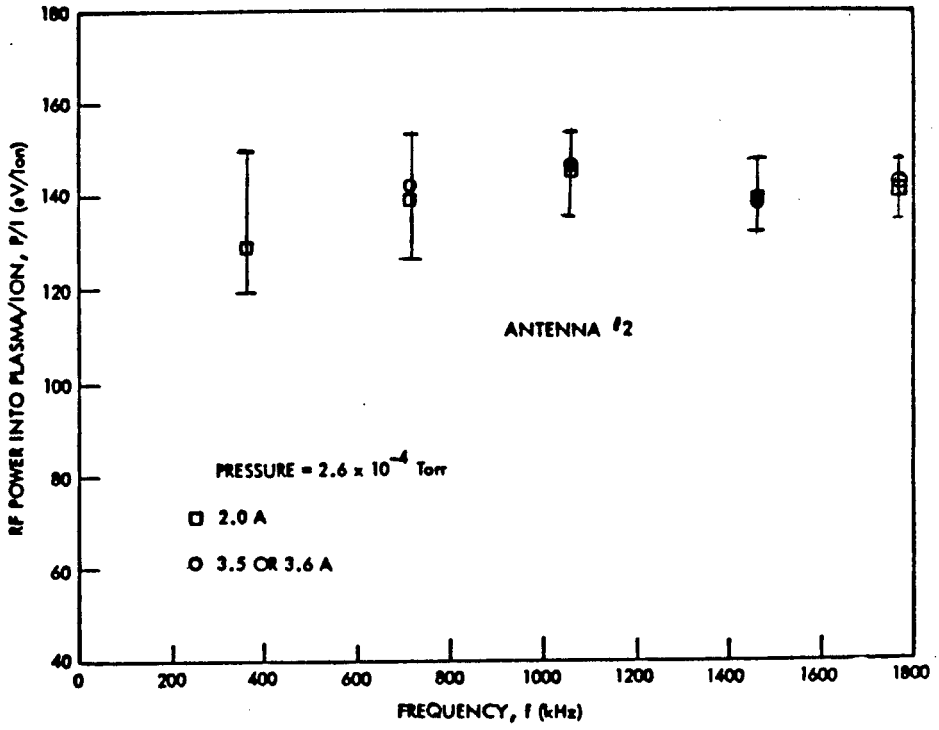

Figure 3-5. Discharge losses were independent of rf frequency.

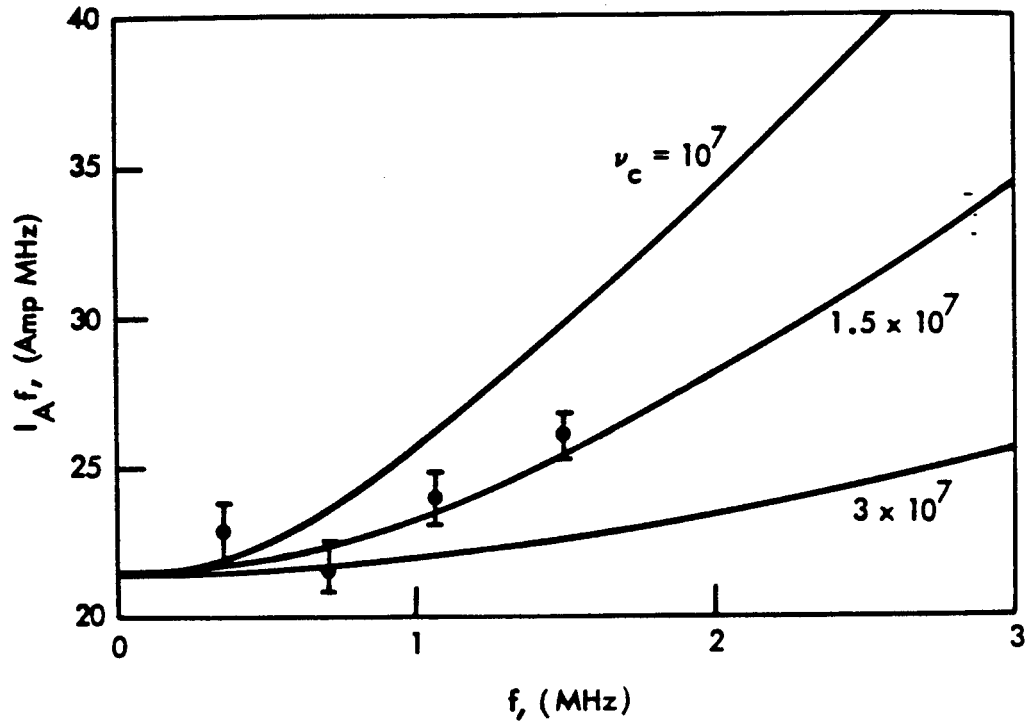

Figure 3-6. Antenna current times frequency versus frequency

The observed frequency dependence of the antenna current is seen to agree reasonably well with the theoretical form given by equation (3.1) with an effective collision frequency of

$$\nu = 1.5 \times 10^7/\text{sec.}$$

Combining (3.1) and the frequency dependency of the antenna resistivity (i.e., the skin effect), the frequency dependence of the antenna resistive power can be expressed as

$$P_A = I_A^2 \, R_A \propto (\nu/\omega)^{3/2}_5 + (\omega/\nu)^{1/2} \qquad (3.2)$$

which has a weak minimum at a frequency

$$\omega = \sqrt{3}\ \nu \qquad (3.3)$$

Figure 3-7 is a plot of P_A normalized to the minimum value, and shows that the minimum is very broad, thus allowing a considerable range over which the rf frequency may be chosen. For the experimentally determined

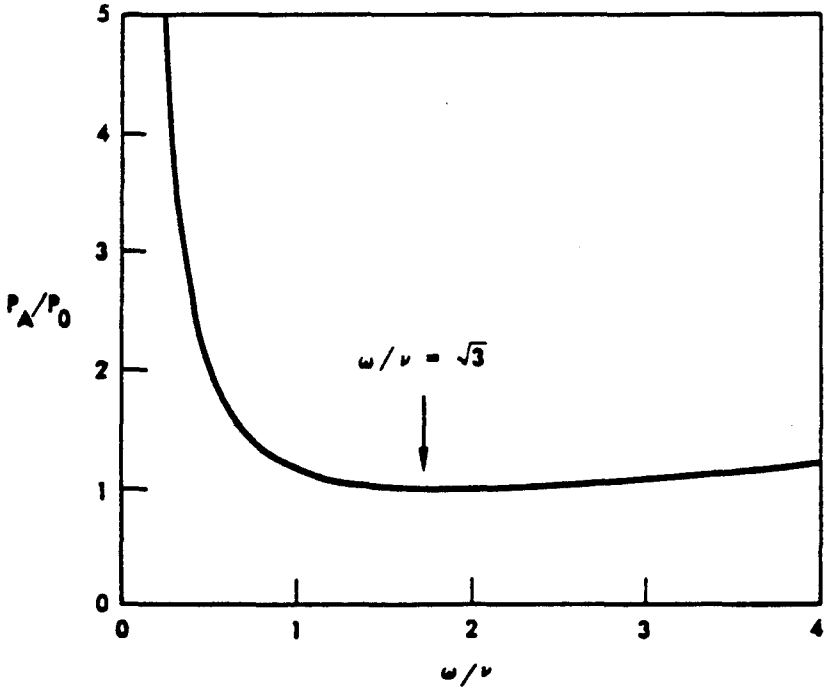

Figure 3-7. Normalized antenna power versus quotient of driving and collision frequencies

value of $\nu \simeq 1.5 \times 10^7$/sec., equation (3.3) predicts a frequency of approximately 4.1 MHz for minimum antenna losses. For operation at a frequency of 1.5 MHz, equation (3.2) predicts antenna losses to be about 60 percent higher than that at the minimum. However, measured antenna losses at a frequency of 1.5 MHz represent only 5 percent of total discharge power. The dependence of overall discharge efficiency on choice of frequency is extremely weak over a wide range.

3.3.2 Beam Extraction Measurements

The Axial Line Cusp Radio Frequency Induction thruster was operated with beam extraction in a two-week series of tests at the Tank 5 facility at NASA Lewis Research Center. The purpose of these tests was to demonstrate its feasibility and to characterize the operation of this first experimental model of a multicusp rf thruster under conditions of continuous ion beam extraction. An important goal of the tests was to determine to what degree test results, obtained without beam extraction, could be extrapolated to actual thruster operation. The rf frequency for this

series of tests was 1.5 MHz. Following a one-week series of tests, the ceramic magnets were replaced with samarium cobalt magnets which approximately doubled the magnetic field strength.

Perhaps the most significant result of this series of tests was that no problems in beam extraction peculiar to rf discharge operation, rather than dc discharge operation, were encountered. Performance of the thruster with the original ceramic magnet configuration is illustrated in Figure 3-8, which plots discharge losses (eV/ion of beam, with rf circuit losses subtracted out) versus propellant utilization with mass flow as a parameter. As illustrated in Figure 3-9, operation with samarium cobalt magnets give only very slightly improved performance.

A comparison was made of the determination of discharge losses with and without beam extraction, utilizing the samarium cobalt magnets. For measurements without beam extraction, the screen and accel grids were electrically connected and biased at -40 volts with respect to the thruster walls, which were held at ground potential. It was found that when the ion current collected by the screen and accel grid combination was multiplied by a factor of 0.7 to adjust for ion losses to the screen during normal beam extraction, then the discharge losses with and without extraction were the same to within experimental error for propellant utilizations of less than about 0.4. At high utilizations, as expected, the discharge loss figures obtained without beam extraction were significantly lower than with extraction; this is due to recycling of ions recombining on the screen. Indeed, without extraction, an apparent utilization of greater than one could easily be obtained. Data comparing results at flow rates of 6.6 amp and 3.9 amp equivalent are illustrated in Figure 3-10. It should be noted that the utilization efficiency is influenced strongly by the perveance or ion extraction capability of the accelerator grids and that SHAG optics are inherently limited in current density because of the smaller accelerator holes.

3.3.3 Areas for Performance Improvement

A series of detailed probe measurements of electron density and temperature profiles in the thruster were undertaken at the TRW facility. The purpose of the tests was to obtain additional data to aid in the interpretation of the discharge loss characteristics of the thruster and thus provide direction for improvement of these characteristics.

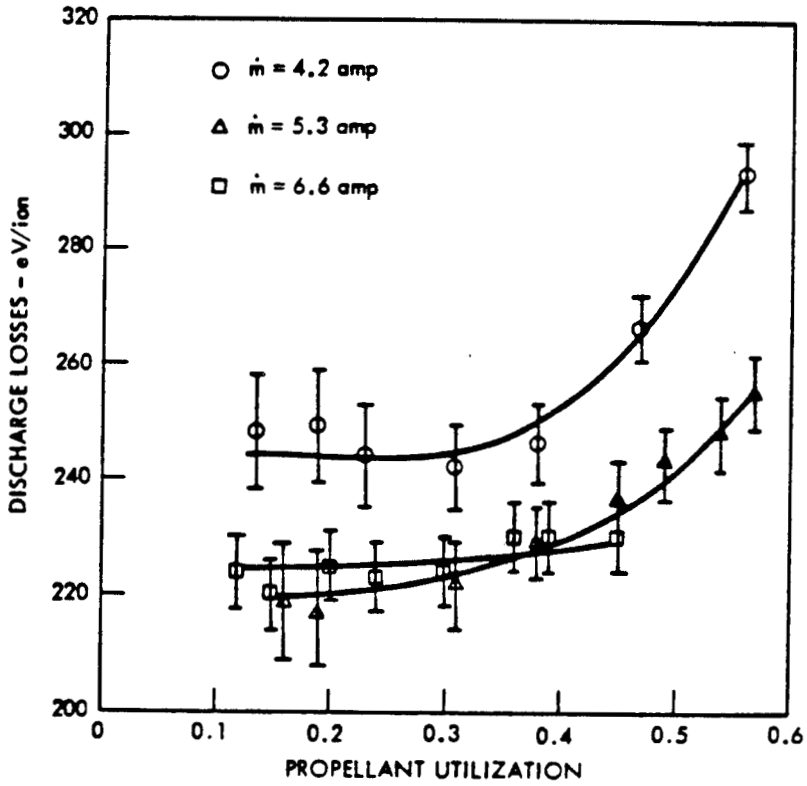

Figure 3-8. Thruster performance with ceramic magnets (1.5 KG) at flow rates of 4.2, 5.3, and 6.6 ampere equivalent Argon flow rates.

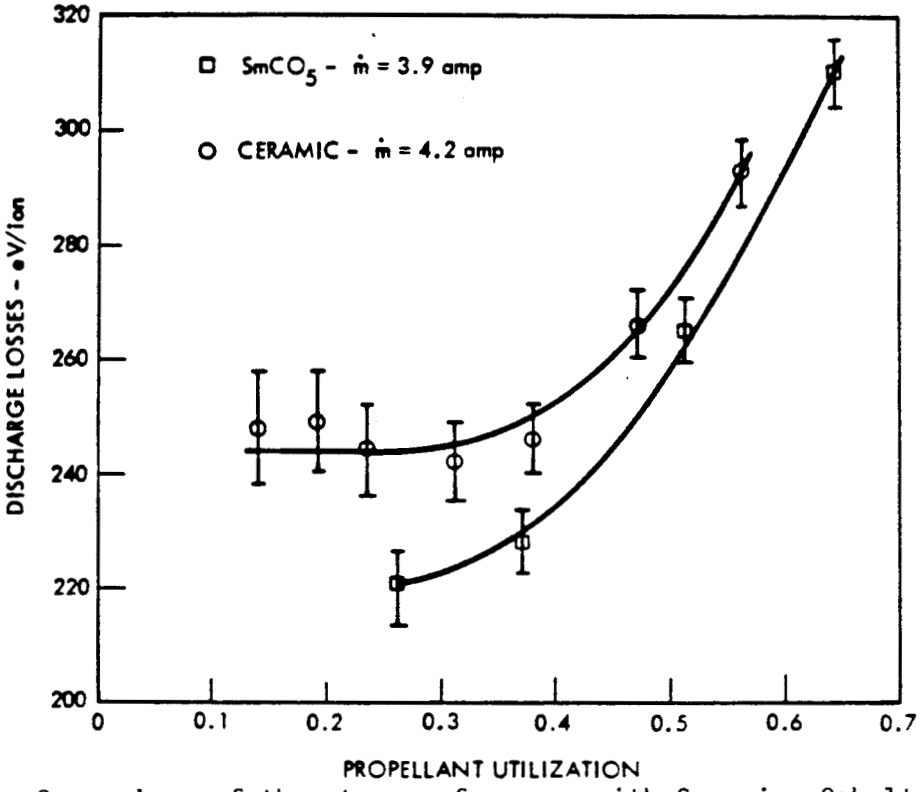

Figure 3-9. Comparison of thruster performance with Samarium Cobalt and ceramic magnets at mass flow rate of 4.1 ampere equivalent.

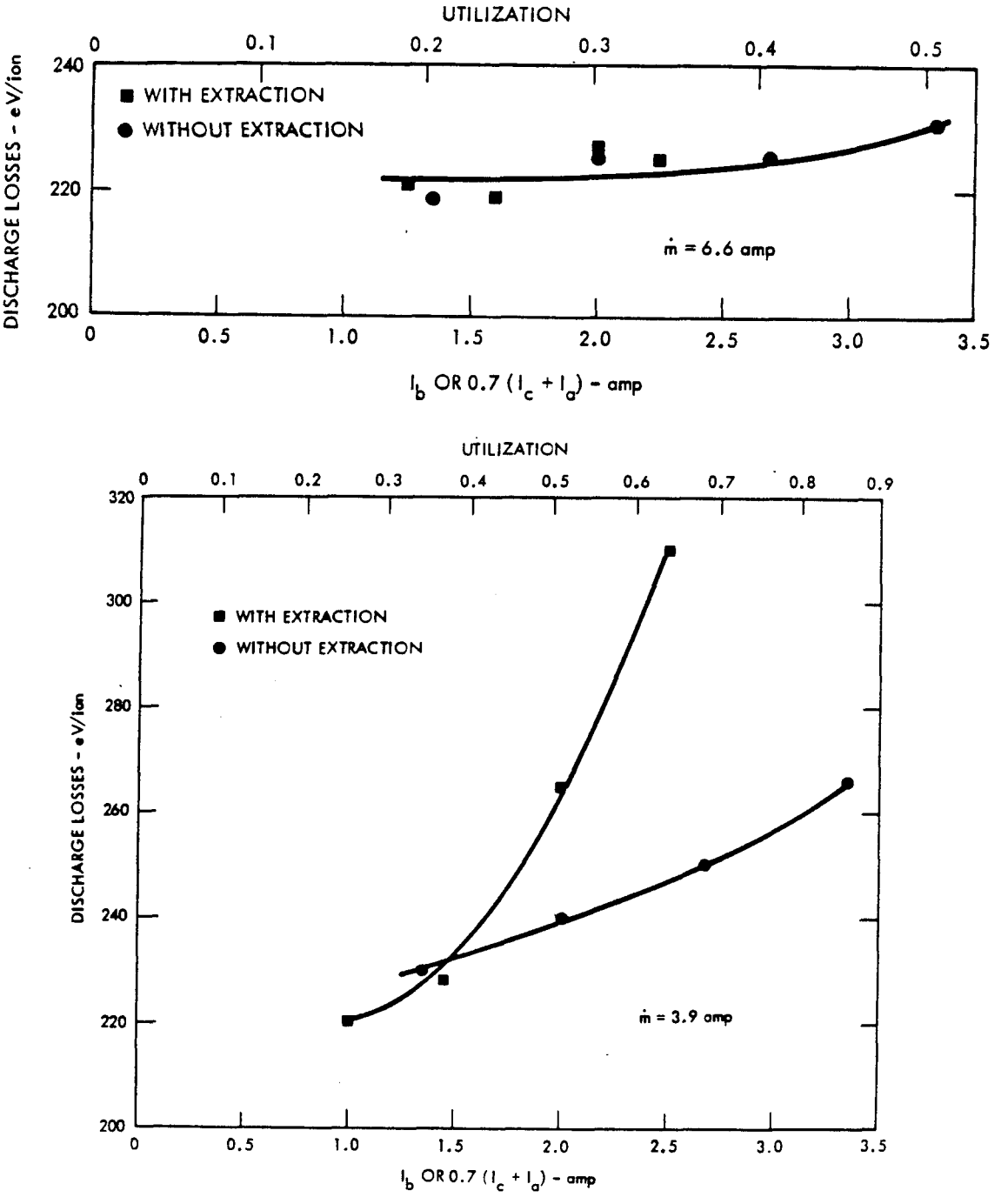

Figure 3-10. Comparison of discharge losses measured with and without beam extraction, as a function of beam current or equivalent beam current, obtained by correcting the collected screen plus accel current by the factor 0.7.

The results of these tests indicated that while the electron temperature was greatly reduced in the region close to the wall between the magnets, the electron density was not. It was concluded that the magnet configuration used did not possess sufficient magnetic flux to affect the desired reduction of ion losses between the magnet rows.

For optimum grid performance and high propellant utilization, the ion current density profile at the screen grid should be as flat as possible. The measured profiles in the Axial Line Cusp RFI Thruster, as shown in Figure 3-11, were far from optimum, being close to parabolic rather than flat; optimizing the beam profile is an area for potential improvement of the performance characteristics.

3.3.4 Conclusions

The first series of tests with an RFI Multicusp Thruster demonstrated the basic feasibility of the concept for thruster applications. Very efficient coupling of rf power to the discharge was demonstrated, with antenna circuit losses of about 5 percent. The independence of discharge losses on rf frequency was shown over the range 0.35 MHz to 1.75 MHz and antenna circuit losses were studied over the same range. From an extrapolation these results it can be concluded that the optimum rf frequency lies in the range 1.5 MHz to about 8 MHz, but that within this range the overall effect on discharge efficiency is probably less than 10 percent.

Performance characteristics of the thruster during beam extraction were promising, but would require considerable improvement to be competitive with state-of-the-art hollow cathode thrusters. Minimum discharge losses were approximately 220 eV/ion, while the knee of the performance curve occurred at approximately 60 percent utilization and 250 eV/ion. Following an analysis of the discharge efficiency results as well as the plasma profile measurement results, it was concluded that the primary area for improvement of performance was in the magnetic geometry.

3.4 AZIMUTHAL LINE CUSP RFI THRUSTERS

3.4.1 Configurations

Four azimuthal cusp RFI plasma generators which we will label as AZIM I-IV were fabricated and tested during the 1982-83 phase of the program. AZIM I, II, and III were comprised of different magnet configurations

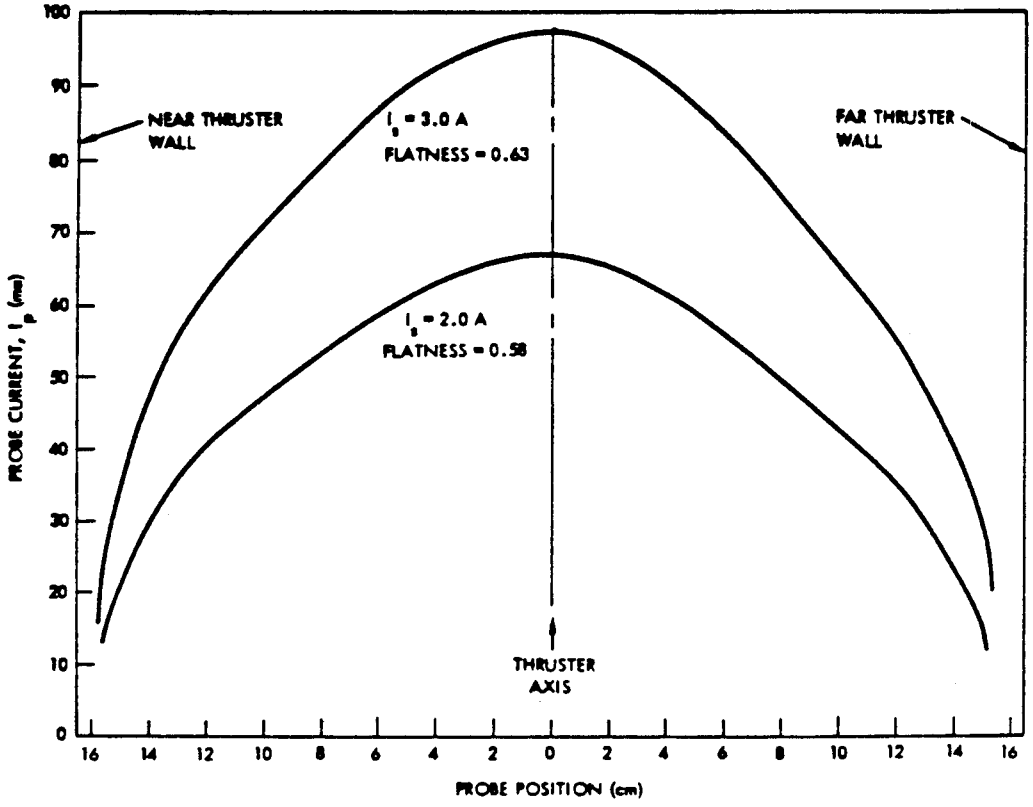

Figure 3-11. Probe ion current traces near screen electrode inside rf source

mounted on the same thruster shell. This shell consisted of a 33 cm diameter, 30 cm long, 1 mm thick stainless steel cylinder, closed at the upstream end by a 2 mm thick stainless steel sheet. At the other end of the cylinder in place of extraction optics, a 0.25-inch thick perforated copper "extraction plate" was mounted. The extraction plate was electrically isolated from the shell and was normally biased at 40 volts negative with respect to the shell in order to obtain a measurement of the total ion current flowing to the extraction plane. This plate could be mounted at any desired position within the cylinder; in this way the thruster length could be variabled from a few centimeters up to 30 cm. As many as 12 one-half inch diameter copper discs were mounted at various positions on the inside of the extraction plate to serve as ion current density probes. The discs were insulated from the plate by thin mica sheets and were capable of being independently biased.

The backplate magnet configuration was identical for all four azimuthal cusp thrusters. The configuration, shown schematically in Figure 3-12, consisted of two rings and one disc of samarium cobalt magnets mounted on a soft iron plate. In the AZIM I configuration shown in Figure 3-13, three rings of samarium cobalt magnets were mounted on the cylindrical shell. Each ring consisted of 24 1.0 x 1.0 x 0.50 inch magnets equally spaced about the perimeter; this resulted in an inter-magnet spacing of 0.7 inches. A 1.0 inch wide by 0.125 inch thick mid-steel ring was mounted inside the thruster shell and was coaxial with each ring of magnets. This internal pole piece served to smooth out the magnetic field strength in the azimuthal direction. With the pole piece in place, the azimuthal variation in field strength for any fixed radial and axial coordinates was measured to be less than 10 percent. The peak field strength at the pole piece was approximately 2.0 K gauss. As indicated in figure 3-13, the outer poles of the ring magnets were magnetically connected by 0.25 inch thick, 1.0 inch wide pole pieces.

For the second azimuthal cusp configuration, AZIM II, the internal pole pieces were removed and the number of magnets in each of the three rings on the thruster cylinder was increased to 41, such that adjacent magnets were in contact. This change increased the peak magnetic field strength at the thruster wall to about 4.0 K gauss.

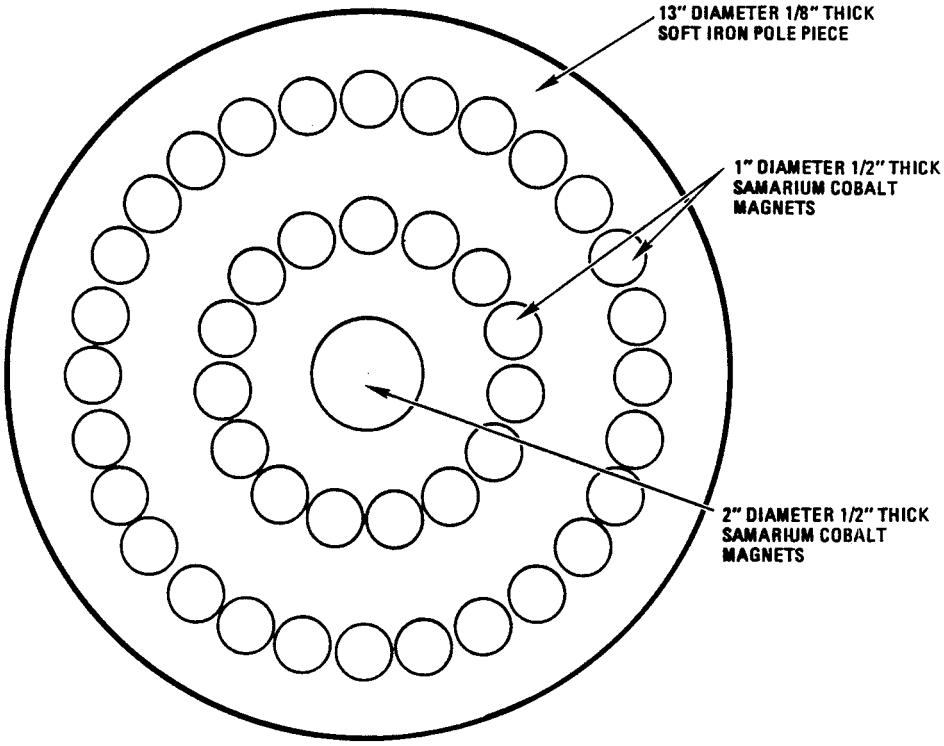

Figure 3-12. Backplate magnet configuration for all Azimuthal Cusp Thrusters

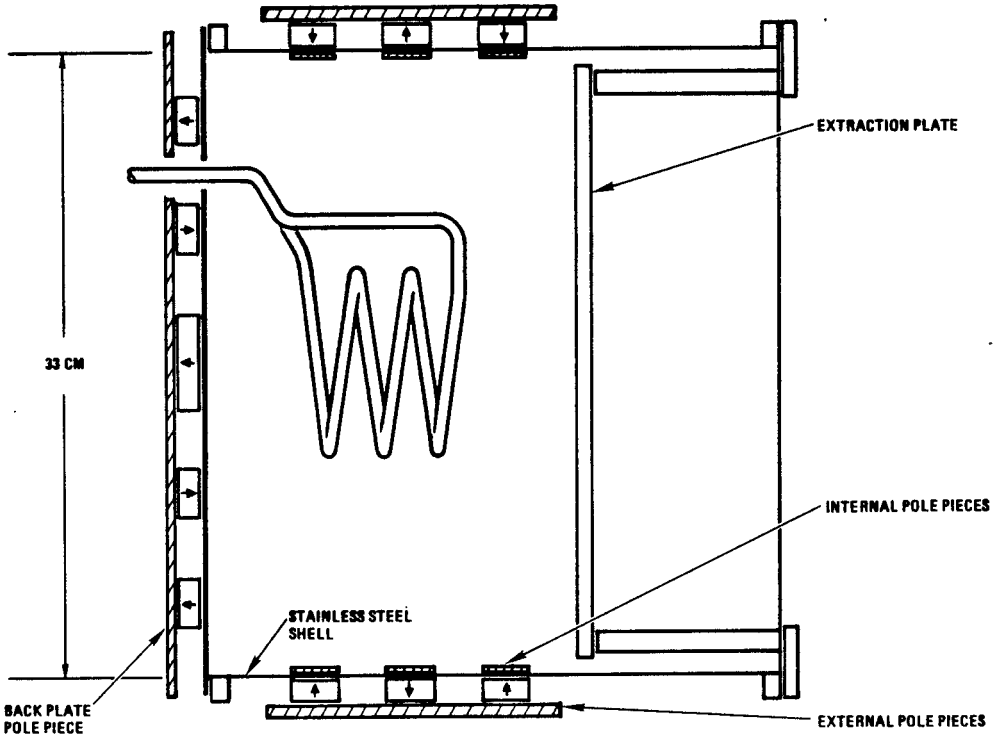

Figure 3-13. AZIM I Configuration

The third azimuthal cusp configuration was the same as AZIM II but with a 14 cm diameter, 8 cm long electromagnet added-on axis, just behind the backplate. This modification enabled the addition of a weak (<100 gauss) divergent magnetic field over the volume of the plasma.

An entire new thruster assembly, shown schematically in Figure 3-14, was constructed for AZIM IV. The backplate configuration was identical to that of the first three configurations, but the outer cylindrical shell was constructed of 0.25 inch thick mild steel, serving as both mounting structure and pole-piece for the magnets. Five rings of samarium cobalt magnets were mounted on the inner surface of the cylinder, with adjacent magnets in each ring in contact with each other. The magnets in the back three rows were 1.0 x 1.0 x 0.5 inch, while those in the front two rows were 0.50 x 1.0 x 0.50 inch, where the dimensions are given in the axial, azimuthal and radial directions respectively. The spacing between rings was greatly reduced from the first three azimuthal cusp configurations in order to increase the magnetic field between the cusps. Finally a 1 mm thick copper liner was mounted inside the magnet assembly to protect the magnets from direct contact with the plasma.

The rf power and measurement system for all thrusters was of the same general configuration as used for the axial line cusp thruster (Figure 3-2), and the operating frequency was always 1.4 - 1.5 MHz. As improvement of the ion current density profile was a major goal of this phase of the program, the previously described diagnostic technique of mounting disc probes at the extraction plane was used on all thrusters. AZIM I, II and III were operated on the same TRW test stand as the axial line cusp thruster discussed in Section 3.3. AZIM IV was operated on the TRW Energy Research Center ion source test chamber. At this facility, all rf system and probe data was digitized and recorded with an online computerized data acquisition system.

3.4.2 Efficiency Measurements

Discharge loss results for the four azimuthal cusp configurations are summarized in Table 3-1. Also included for comparison are results for the axial line cusp thruster. For each case, three values of discharge losses are shown. For the two "non-extracted" values, the ion current was the current collected by the biased extraction plate. The measured antenna circuit resistive losses have been subtracted out in the first of these two

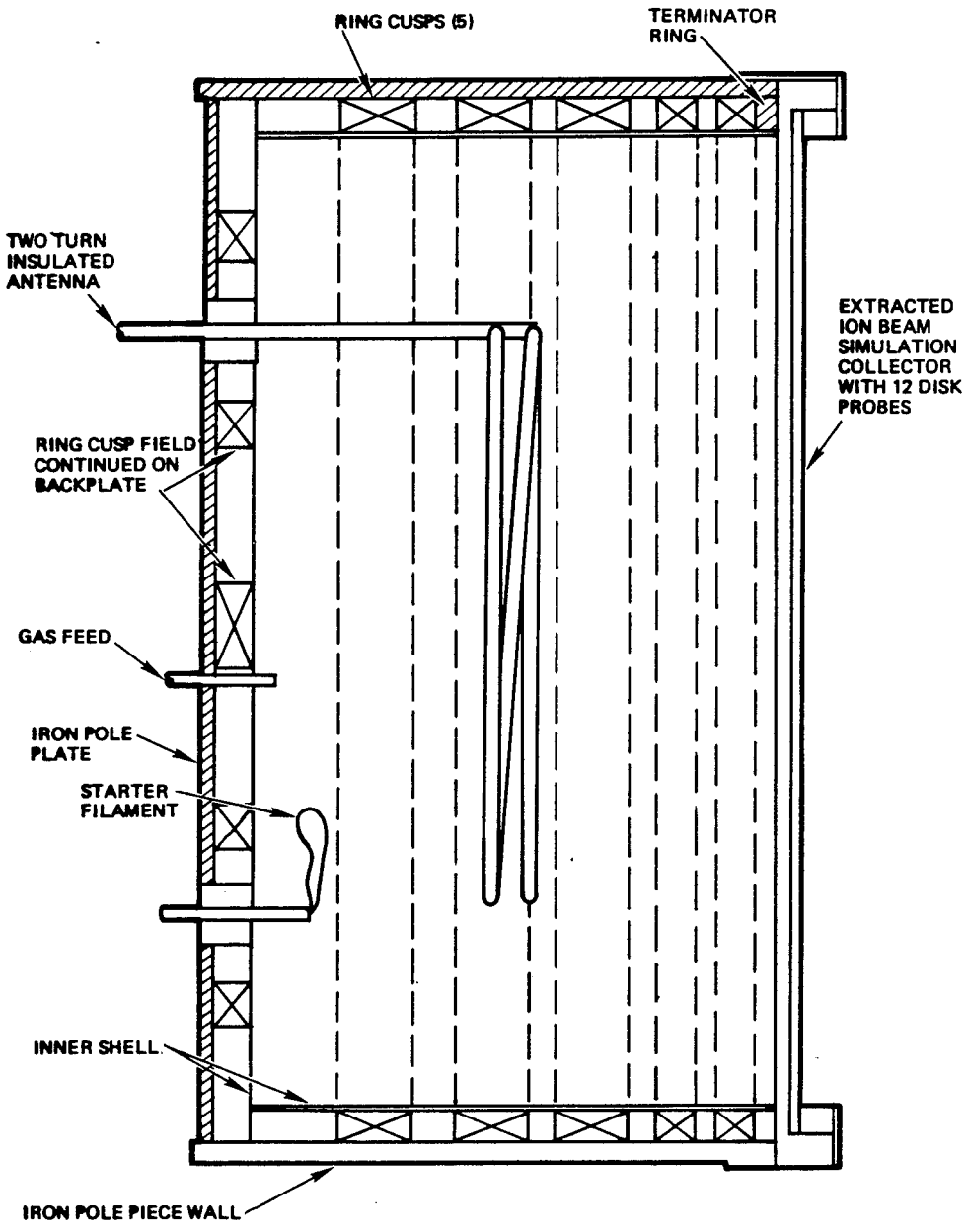

Figure 3-14. Schematic of the AZIM IV Configuration

Table 3-1. Summary of RFI Thruster Discharge Loss Results

Model	Date	Discharge Losses- eV/ion Non-Extracted W/O RF Losses	Non-Extracted W/ RF Losses	Assuming 90% Optics
AXIAL	7/81	143	155	172
AZIM I	8/82	140	150	167
AZIM IIA	9/82	122	134	149
AZIM IID	9/82	117	129	143
AZIM III	11/82	122	134	152
AZIM IV	6/83	100	108	120

values but are included in the second. It is likely that resistive losses may be reduced somewhat by improvement of antenna design and by optimization of the operating frequency. The final value for discharge losses represents losses per beam ion and assumes a screen grid which is 90 percent transparent to the incident ions, a value which appears to be typical for state-of-the-art two grid systems. Antenna circuit losses are included in this value. All experimental data for this table was obtained at an operating pressure of about 4×10^{-4} torr of Argon, in which pressure regime discharge losses are found to be rather pressure independent, and with between 3 and 5 amperes of ion current drawn to the extraction plate.

Discharge losses for AZIM I were not significantly lower than for the axial line cusp thruster and the unit was tested only minimally before conversion to AZIM II. AZIM II was first operated with a chamber length of 20 cm (IIA), so that all chamber dimensions were identical to the axial line cusp thruster. Performance was found to be improved by about 15 percent over the axial line cusp thruster. It was decided to investigate this configuration further. Several antenna designs were tested and the thruster was operated at two other lengths: 15 cm and 12 cm. Discharge losses at these two lengths were nearly identical and represented a slight (4 percent) improvement over the 20 cm length. AZIM IID in Table 3-1 is the 12 cm depth

thruster and represents the best performance for AZIM II. Dependence of discharge losses on gas pressure for AZIM IIA is illustrated in Figure 3-15.

The attempt to further reduce discharge losses by imposing a divergent volume magnetic field on the thruster was not particularly successful, but the results indicate that future work in this area may be fruitful. As illustrated in Figure 3-16, discharge losses show a minimum as a function of applied field. However, for the AZIM III configuration, minimum discharge losses were only 5 percent less than the value for zero applied field.

Based on the results obtained with AZIM II, a discharge chamber length of 16 cm was chosen for AZIM IV. From the AZIM II results, shorter lengths do not significantly reduce discharge chamber losses, but would undoubtedly reduce propellant utilization. Though the backplates were identical in AZIM II and IV, the AZIM IV design employed significantly stronger magnet fields on the cylindrical surface, particularly in between the cusps. Discharge losses were found to be reduced significantly, to a minimum of 100 eV/ion, not including rf circuit losses. Dependence of discharge losses on gas pressure for AZIM IV is illustrated in Figure 3-17, for an extraction plate ion current of 5 amperes. The performance improvement of AZIM IV over AZIM II was obtained through an increase of the cylinder wall magnetic field strength only. Extrapolating from the results, it is estimated that a similar increase in the backplate field strength could affect a discharge loss reduction of another 10 eV/ion.

3.4.3 Plasma Density Profiles

The second area identified for improvement following the axial line cusp development phase of the program was the ion current density profile at the extraction plane. As noted in Section 3.3, the axial line cusp thruster profile was close to parabolic. Such a profile reduces propellant utilization from what would be expected for a flat profile, and does not allow efficient matching of the source plasma to the ion optics.

Current density profiles were examined in AZIM I - III, but no attempt was made to improve the profile as the emphasis was on reducing the discharge losses. Profiles for these devices were similar to the axial line cusp thruster, as illustrated in Figure 3-18 (a and b) for AZIM I and AZIM II. An attempt to improve the current density profile was included in the

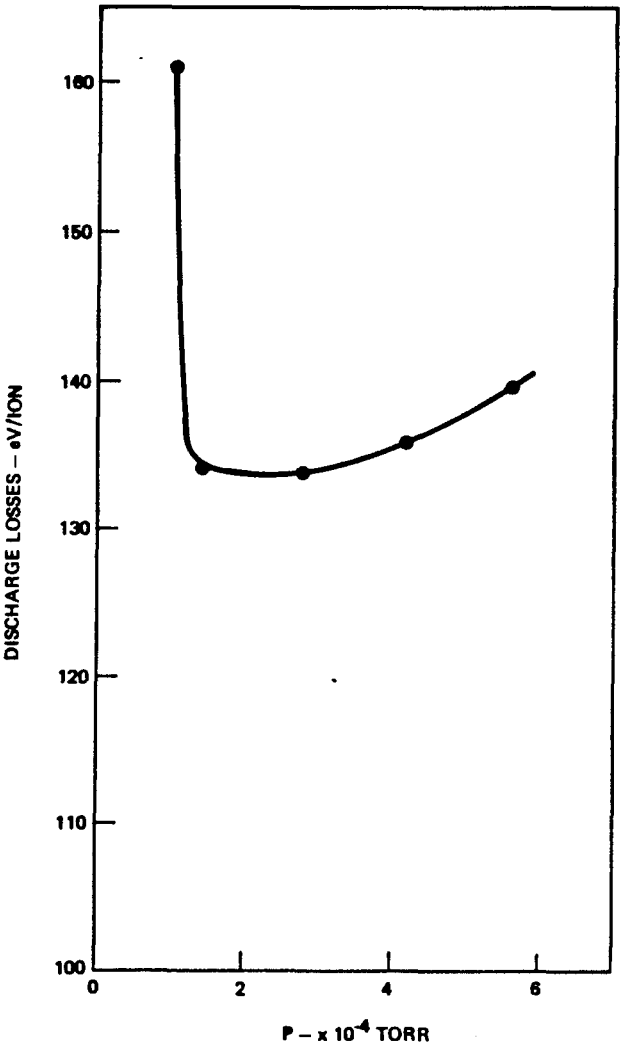

Figure 3-15. AZIM II Discharge losses as function of gas fill pressure at 4 amps ion current

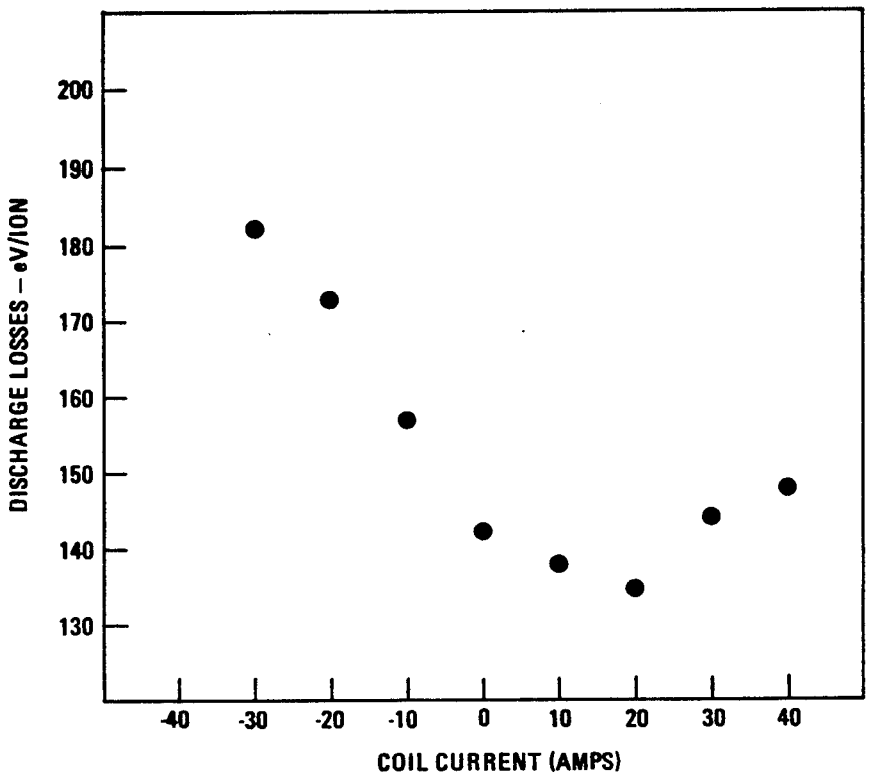

Figure 3-16. Discharge losses as a function of electromagnet current in AZIM III. Extraction plate ion current was 4 amperes.

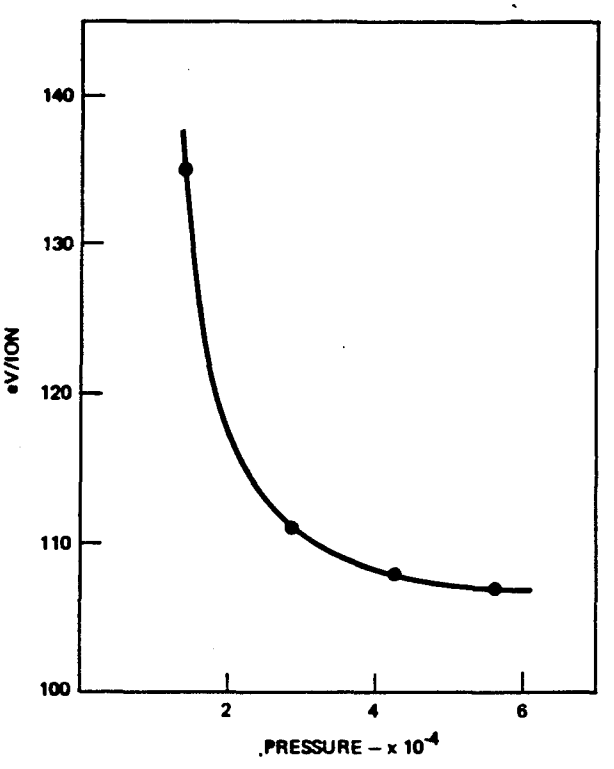

Figure 3-17. AZIM IV Discharge losses as function of gas fill pressure measured at 5 amps ion current

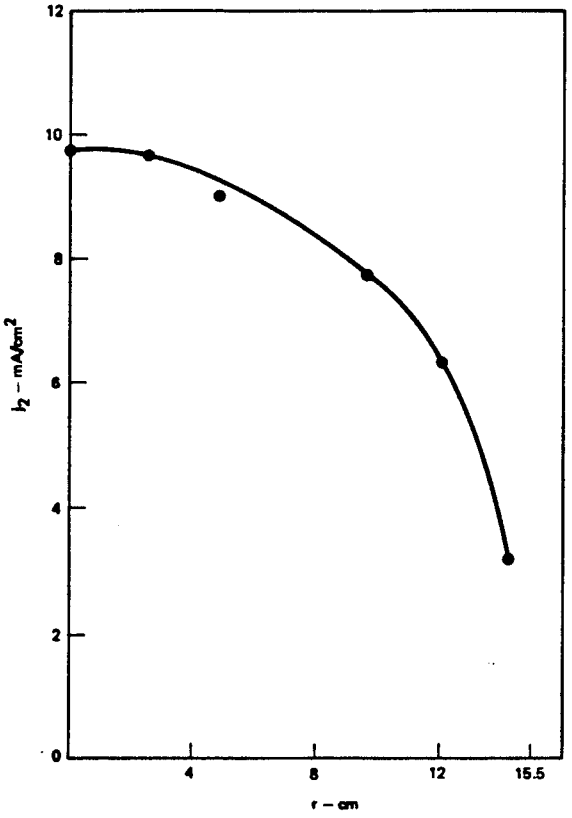

Figure 3-18a. AZIM I ion current density profile Argon fill pressure was 2.7×10^{-4} torr

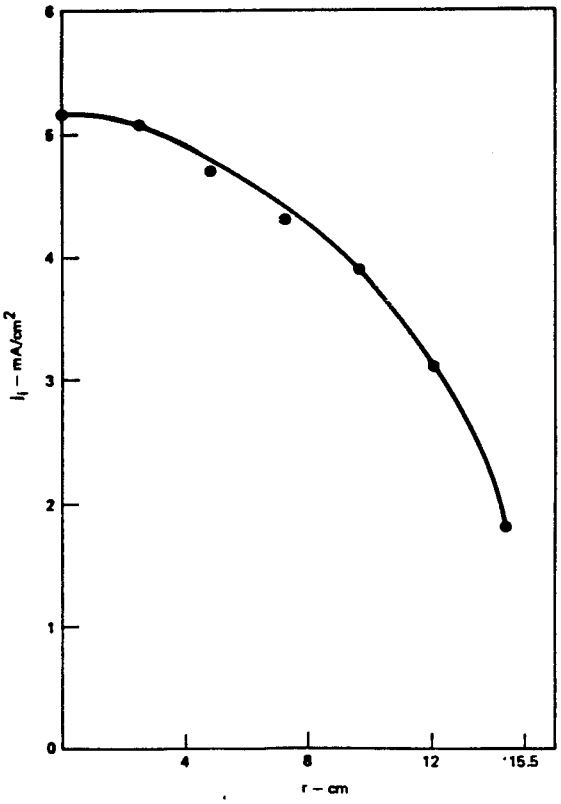

Figure 3-18b. AZIM II ion current density profile Argon fill pressure was 2.8×10^{-4} torr

01-088-84

design of AZIM IV. It is well known that in multi-cusp discharge chambers, the plasma density profile is largely determined by the gradient in the magnetic field. Closer magnet spacing provides steeper magnetic field gradients, and therefore, flatter density profiles but also results in greater ion losses to the walls. An innovative design feature employed in AZIM IV is a magnet spacing which can be varied as a function of distance from the extraction plane. For AZIM IV, small and closely spaced magnets were placed near the extraction plane in order to produce a flat ion current density profile at that position, and larger, less closely spaced magnets are used at the rear of the chamber to minimize losses to the wall. As illustrated in Figure 3-19, profiles were greatly improved in this configuration, and further development of this design technique appears warranted.

3.4.4 Discussion and Summary

We have presented the results of a series of thruster configurations employing permanent magnets arranged in an azimuthal cusp geometry. The permanent magnets surrounding the thruster shell are employed, of course, in an attempt to increase the particle confinement time in the device and, thus, allow ions more of a chance of being extracted to the beam for useful purpose rather than being lost to the walls. When one considers plasma confinement in a cusp magnetic field geometry one imagines plasma particles being channeled along the cusp field and lost at a certain rate which should depend upon the magnetic field strength; transport of the particles across the magnetic field is generally thought to occur at a much slower rate. Thus with this picture in mind, and considering the purpose of the cusp fields, one would assemble an electrically efficient steady-state plasma generator by minimizing the total length of cusps used and by maximizing the field strength of the cusps in order to obtain optimum performance. Other considerations, such as gas utilization and beam flatness, which affect the eV/ion and optics performance must also be kept in mind.

The first experimental 30 cm RFI plasma generator which had ceramic magnets arranged in an axial cusp geometry achieved a minimum eV/ion of ~ 220 eV/ion, as discussed in Section 3.3.2. Tests with the same generator but with the ceramic magnets replaced by magnets of Samarium Cobalt in the same geometry reduced the eV/ion by only 5 to 10 percent even though the cusp field strength was nearly increased by a factor 2. Subsequent probing

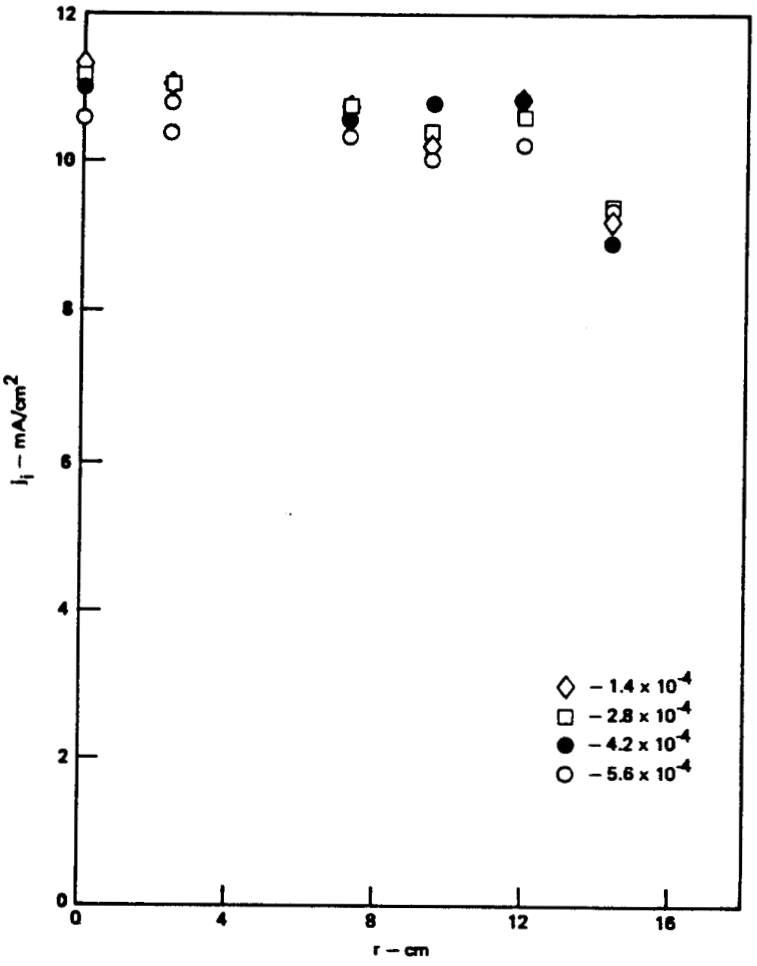

Figure 3-19. AZIM IV ion current density profiles Argon fill pressure

of this configuration indicated that the ion current density near the walls was almost uniform, although the electron temperature at the cusps was considerably higher than that between the cusps. It therefore appears that there is considerable cross field transport of the ions which in turn drag electrons across the field lines with them. The total length of cusps in the device would thus not be the dominant factor affecting efficiency; instead, it may be that the total magnetic flux near the walls is the important factor. To what extent the effects of (1) field line errors, caused by imperfect placement of the magnets or (2) the fact that particle guiding center drift orbits in the axial line configuration terminate at the thruster walls, affect the particle confinement is not known.

It should further be noted that both the propellant utilization and beam profile were rather poor with the axial cusp configuration. Improvements in utilization (and possibly in eV/ion) can be obtained by improving the beam flatness.

The purpose of the experiments described in this Section 3.4 was to improve the thruster efficiency (eV/ion) and the beam profile. As with the ECH thruster described in Section 4.2, the reason for the azimuthal magnet geometry is to close the particle drift orbits which, as just mentioned, terminate at the device walls and extraction plane in the axial line cusp configuration. In addition, this azimuthal geometry allows one to terminate the flux lines nearest the extraction plane in a cylindrically symetric fashion and allows one to incorporate variable magnet spacing in the axial direction.

The idea behind the AZIM I configuration was to provide, by the use of mild steel between the magnets and the plasma, a smooth surface field very near the walls of the device and at the same time reduce the volume field strength. Sufficient magnetic flux near the walls would hopefully increase the confinement. However the eV/ion and "beam" profile of this configuration proved to be about the same as axial configuration. Removal of the internal mild steel and an increase in the number of magnets, such that three continuous rings of magnets surrounded the thruster shell (AZIM II), reduced the eV/ion by about 15 percent. The "beam" profile was, however, still poor; no attempt at terminating the magnet ring nearest the extraction plane or varying the relative position of the magnet ring and

extraction plane had been made at this time. However, variations in the axial length of this configuration by almost 50 percent resulted in only very small (~ 4 percent) variations in the eV/ion, which may lead one to suspect that losses at the backplate are not inconsequential.

The addition of a variable electromagnet on the backplate (AZIM III) which superposed a mildly diverging volume magnetic field on the AZIM II configuration did not improve the eV/ion but could cause a considerable increase in discharge losses which may have been due to alterations of the field structure near the backplate or to field changes in the weakly magnetized central volume of the device. Other experiments performed at TRW but not described here have shown that substantial changes in the beam profile can be obtained by the superposition of a weak (~ 2 to 5 gauss) volume field.

The final configuration described and tested (AZIM IV) had a close magnet spacing between adjacent azimuthal rings which resulted in higher field strengths in the regions between the magnets. Magnet rings of larger width were used near the backplate to increase the magnetic flux, while smaller width magnet rings together with a terminating soft iron ring were used near the extraction plane. The result for this geometry was discharge losses of 100 eV/ion and a beam flatness of 90 percent or better.

The development of the RFI plasma generator has demonstrated continuous improvement in the eV/ion from the 220 eV/ion value obtained with the first experimental model to a value of about 100 eV/ion obtained with the AZIM IV configuration. The theoretical minimum obtainable value is probably 50 to 70 eV for Argon. Improvements in the beam profile have also been substantial during the course of this program. The optimization of propellant utilization and the demonstration of the thruster durability and reliability awaits testing under pulsed and long term continuous beam extraction operation.

4. ECH THRUSTER DEVELOPMENT

4.1 INTRODUCTION

Electron cyclotron resonance heating (ECH) at microwave frequencies has been employed for many years for the production and heating of plasmas. Applications for ECH range from thermo-nuclear fusion research[1,2] to electric propulsion[3].

A typical magnetic field geometry for ECH applications is the magnetic mirror geometry shown in Figure 4-1. Here microwaves generally of wavelengths much less than the vacuum vessel dimensions are launched by simple antennae into the chamber which serves as an overmoded, high Q cavity. The microwave frequency, ω_μ, is chosen to match the local electron cyclotron frequency, $\omega_{ce} = eB/m_e$, on some surface between the mirror throat (that is, the maximum B field strength) and the midplane (the minimum B field region). Electrons which pass through this resonance surface are heated by the local microwave electric fields. These energetic electrons, whose guiding centers are constrained to move along the flux lines, make ionizing collisions with the background neutral gas and can thus create a plasma over the entire volume composed of those flux lines which intercept the resonant heating surface. By virtue of invariance of their magnetic moment, charged particles are confined by the magnetic trap of the mirror field and as a consequence a plasma discharge is easily initiated in this mirror geometry at very low microwave power levels and at very low ($<10^{-5}$ torr) background neutral gas pressures.

Once a plasma has been produced one must be concerned with the ability of the microwaves to propagate through the plasma and reach the resonant heating surface in order to sustain the discharge. For the special case in which the electromagnetic wave vector is purely perpendicular to the plasma filled magnetic field lines, two principal modes of propagation can be identified. These are the ordinary (o) mode, with the electric field parallel to the magnetic flux line and the extraordinary (e) mode with the wave electric field perpendicular to the external B field. The propagation characteristics for the e and o mode are shown schematically in Figure 4-2 as a function of magnetic field strength (ω_{ce}/ω_μ) and plasma density

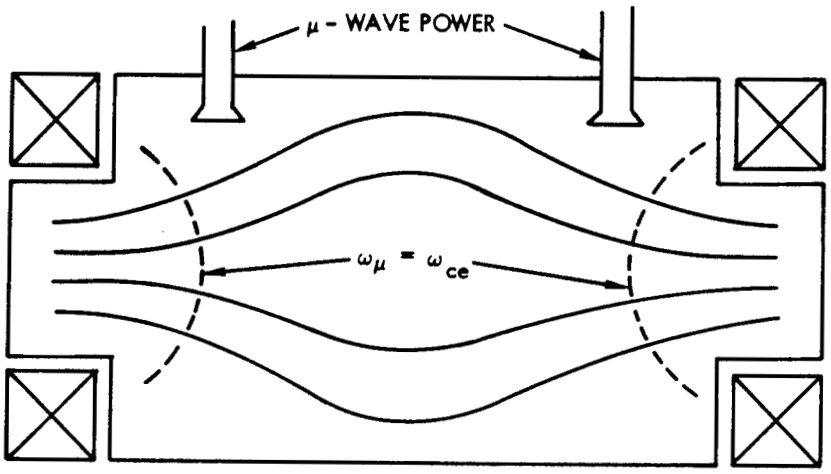

Figure 4-1. Basic Mirror geometry with ECH plasma production

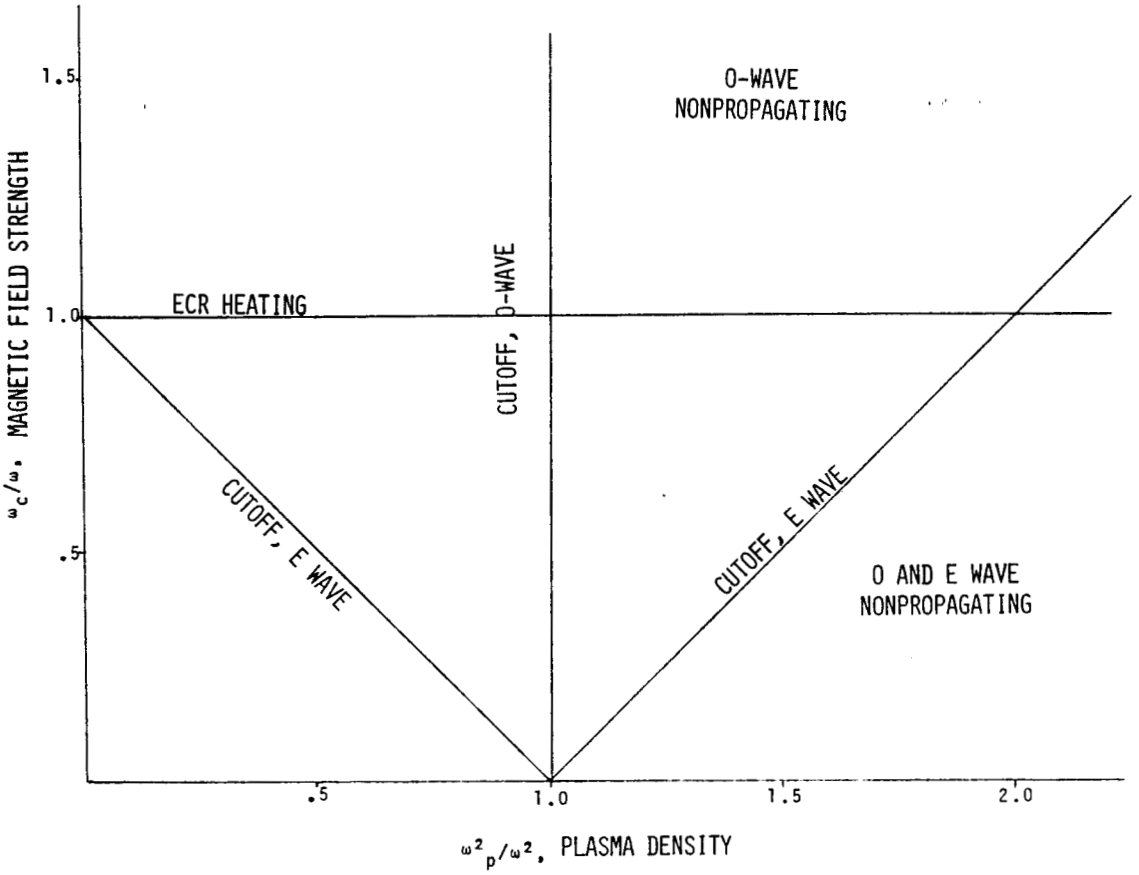

Figure 4-2. Propagation and cutoff regions for ordinary and extraordinary modes for propagation perpendicular to a magnetic field

$(\omega_{pe}^2/\omega_\mu^2) = 4\pi ne^2/(m\omega_\mu^2)$. Waves may be launched from either the high ($\omega_{ce}>\omega_\mu$) or low ($\omega_{ce} < \omega_\mu$) field side and are required to reach the $\omega_{ce}/\omega_\mu = 1$ line in order to resonantly heat electrons. While only the e-mode is strongly absorbed in the neighborhood of the ECH zone, it has a cutoff when launched from the low field side. On the other hand the o-mode can reach the electron resonance zone from either the high or low field side but becomes non-propagating for high plasma densities with $\omega^2_{pe} > \omega^2_\mu$. This latter condition places a criterion on the maximum plasma density that can be obtained at a given microwave frequency, irrespective of the amount of power that is applied, when waves are launched from the low field side. The ordinary wave cutoff condition in turn limits the maximum ion currently density that can be extracted from an ECH-based electrostatic thruster.

4.2 REVIEW OF PREVIOUS TRW ECH THRUSTERS

In previous experimental studies[4] we have investigated plasma production by ECH in two magnetic field geometries. Both geometries introduced microwave power at a frequency of 5 GHz into a 30 cm diameter chamber from a low field launch.

The first magnetic configuration, shown schematically in Figure 4-3 used samarium cobalt permanent magnets arranged in an axial line cusp-configuration. The magnets were placed on the outside of the stainless steel wall that formed the thruster chamber. These magnets which had a pole face field strength of 4.5 K gauss formed the ECH resonance zone for 5 GHz very close to the inside surface of the housing. Representative magnetic field lines of constant B field for this type of magnet configuration are shown in Figure 4-4. It will be seen that a portion of the field lines forms a geometry that is very similar to a magnetic mirror except that the gradient of the field strength is everywhere radially outward (that is, in the -y direction). Thus the plasma, produced by the energetic electrons that fill this mirror region, would preferentially spill radially inward to the central low-field region of the thruster interior from which ions are extracted for thrust. This indeed occurred and a reasonably uniform beam profile was produced. For this axial line cusp configuration the measured discharge efficiency was 250 eV/ion. The maximum ion current

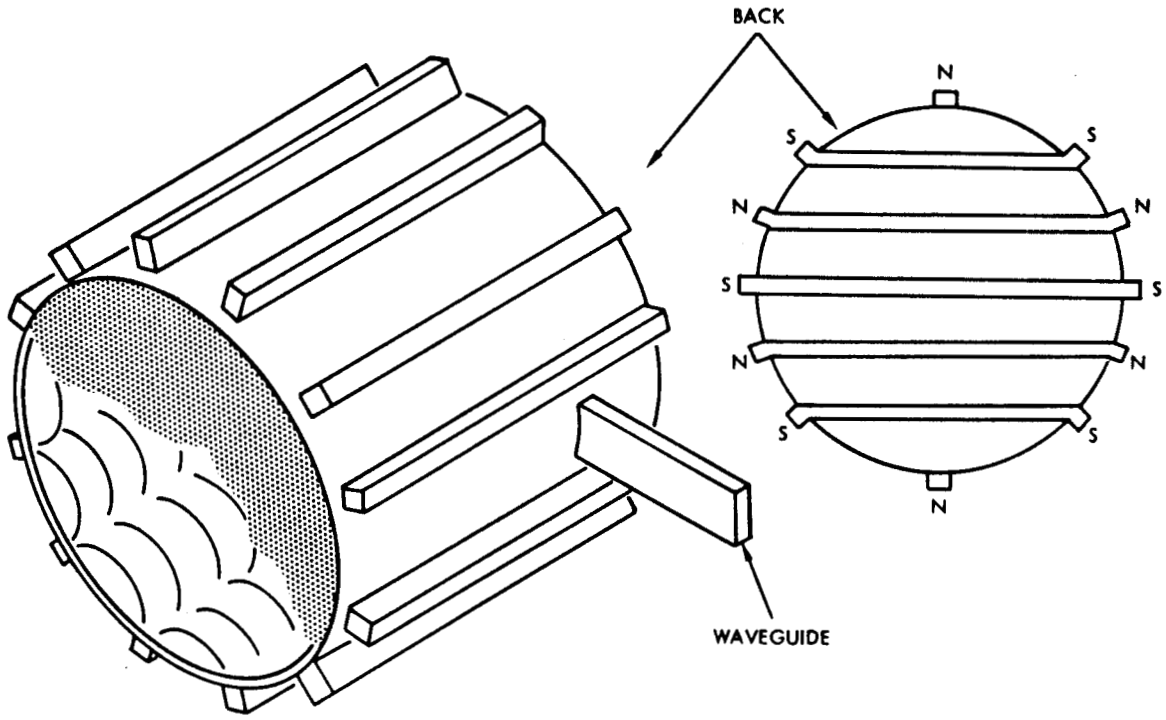

Figure 4-3. Sketch of the ECH source with the axial line cusp magnet configuration

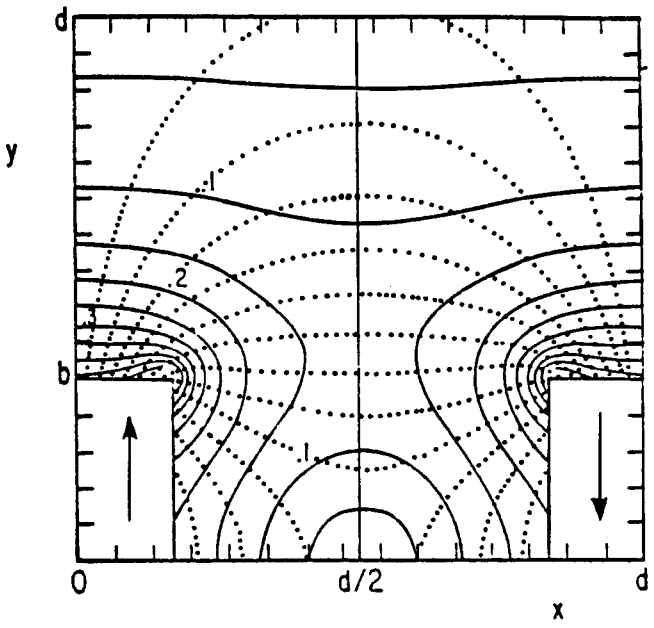

Figure 4-4. Magnetic field lines (dotted) and lines of constant magnetic field (solid) for an infinite periodic array of bar magnets

that could be collected by a biased 30 cm diameter termination plate was about 2.0 amperes and was shown to be limited by the cutoff condition $\omega_{pe} = \omega_{\mu}$.

In an attempt to increase the efficiency of the thruster, that is, to reduce the eV/ion, a second magnet configuration, namely an azimuthal line-cusp, whose geometry is shown in Figure 4-5, was investigated. The same samarium cobalt magnets as in the previous configuration were used. The idea behind the azimuthal arrangement was to close the electron drift surfaces which were open-ended in the axial cusp geometry. The local magnetic field structure would still be very similar to that of Figure 4-4. The resulting efficiency in the azimuthal geometry was indeed improved to a minimum of about 130 eV/ion which would translate to about 185 eV/ion for a 70 percent ion transparency grid set. The maximum ion "beam" current that could be collected by the 30 cm diameter termination plate was 2.5 to 3.0 amperes, again limited, not by available microwave power but by the cutoff density of $n_e = 3 \times 10^{11}$ cm^{-3} for 5 GHz power.

During the course of these experiments some problems became evident which we briefly mention here since they have some impact on an ECH-based thruster concept. The first is that the total microwave power introduced into the thruster would not under all conditions be totally absorbed by the plasma. That is, depending on conditions, 5 to 30 percent of the forward power was reflected back through the power-introducing fundamental mode wave guide. Presumably, by proper impedance matching, this reflected power can be substantially reduced but we were not always successful in doing so with an in-line E-H tuner especially when the thruster was throttled by varying the forward microwave power. Smooth throttling of the ECH thruster was difficult at low power levels as plasma or microwave moding, evidenced by localized electron heating regions and discontinuous jumps in the ion extraction current, occurred.

While the azimuthal permanent magnet configuration resulted in a substantial improvement in the eV/ion value over that obtained with the axial line-cusp configuration, changes in operating parameters to further improve the efficiency of the ECH thruster were difficult to ascertain primarily due to difficulties in probing the microwave filled thruster cavity, in particular, the small mirror-like regions produced by the

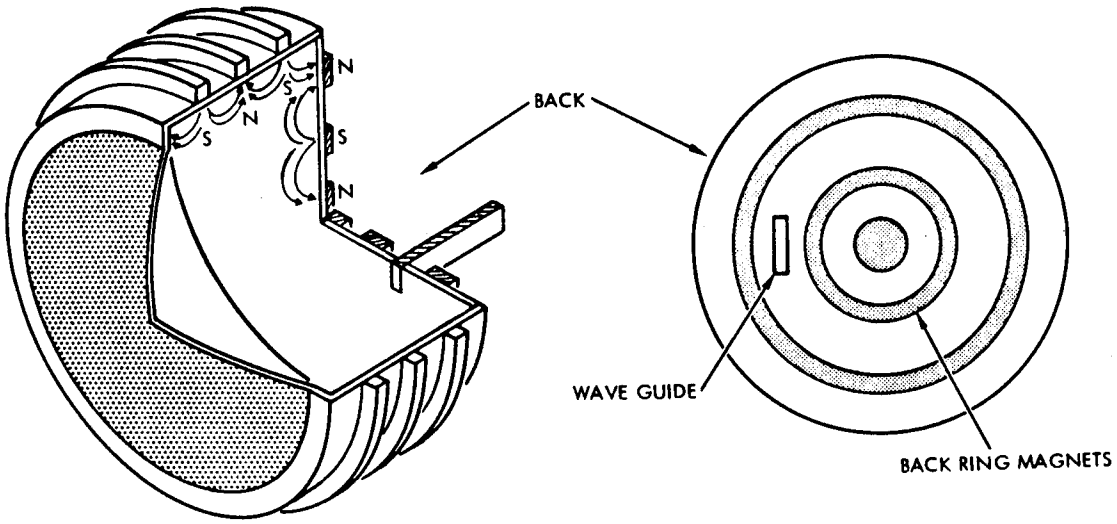

ORIGINAL PAGE
BLACK AND WHITE PHOTOGRAPH

BLACK AND WHITE PHOTOGRAPH

Figure 4-5. Magnet and power feed arrangement for the azimuthal cusp configuration

permanent magnets. In addition, directions for further improvement in plasma production efficiency by varying the magnetic field strength and thus the location of the electron resonance zone could not be gleaned from this permanent magnet device.

It was therefore decided to design, construct and test the ECH thruster concept in a completely different magnetic field geometry, namely in the diverging field of a large solenoidal electromagnet. The geometry and the results of these experiments are described in the following sections.

4.3 SOLENOIDAL B-FIELD ECH THRUSTER

4.3.1 Configuration and Rationale

The new magnetic geometry that was tested under the present effort is shown in a scaled sketch in Figure 4-6. It consists of two 15 cm diameter pancake electromagnets mounted over a 5 cm diameter thin walled antichamber that is an extension of the main thruster housing. The aluminum thruster housing has a length of 20 cm and is terminated at the extraction plane by a 28 cm diameter perforated copper plate which can be biased with respect to the chamber housing to collect the total ion current that would be used for propulsion.

The original set of electromagnets was constructed of closely spaced solid conductor magnet wire. A computer generated plot[5] of the magnetic field lines produced by the two pancake magnets has been superimposed in Figure 4-6. Lines of constant /B/ are indicated in steps of 100 gauss; the mod-B surfaces shown in figure 4-6 are obtained when the magnets are operating at 100 amperes series current.

Since this present ECH thruster operates with microwave power at 5 GHz a minimum magnetic field strength of 1700. Gauss is required in the chamber to produce resonant electron heating surfaces. Microwave power up to 1 kW is again fed by fundamental mode waveguide through a vacuum pressure window into the thruster chamber from a low field launch as shown.

The reasoning behind the construction of this solenoidal-B field geometry and the anticipated operation of the device is as follows. In order to reduce the eV/ion of a thruster, electron and ion losses to the chamber walls have to be reduced and preferably eliminated so that each

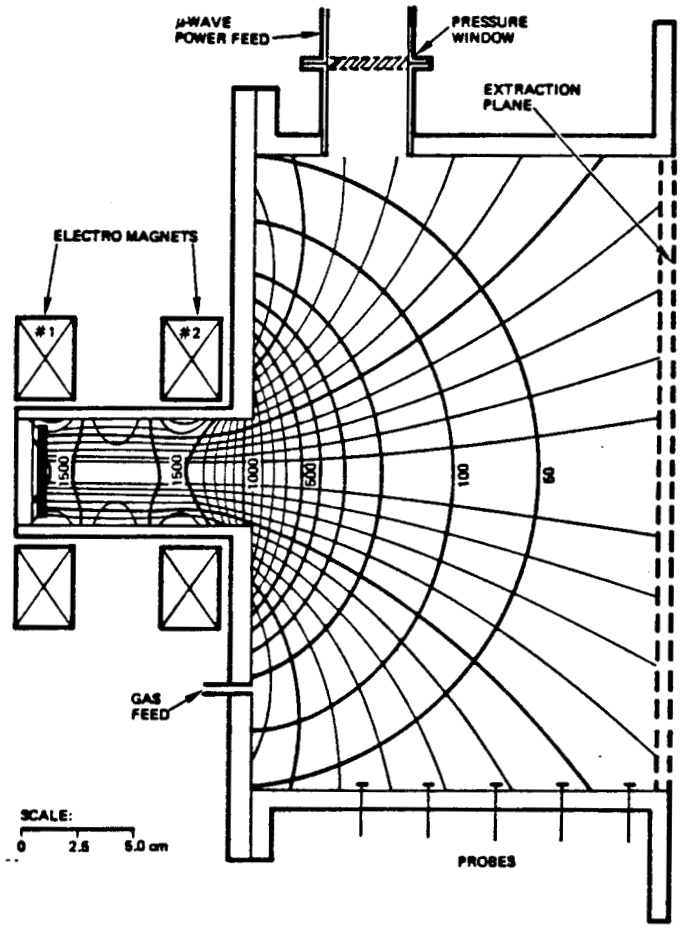

Figure 4-6. Original Solenoidal B-Field Thruster

ion created from an ionizing collision of a neutral atom with an electron is used for beam production. Energetic electrons created by ECH reside only on those magnetic field lines which pass through a resonance zone where $\omega_{ce} = \omega_{\mu}$. Defining the field lines on which heating takes place should, thus, also define the field lines on which plasma is produced. Physical structures or limiters can be placed at appropriate regions to define the field lines on which plasma is produced. These limiters are simply blocks of metal which occupy a spatial volume in which a portion of the fundamental heating surface exists; they thus eliminate electron heating on those field lines which cross this occupied portion of the heating surface. For this solenoidal-B configuration, axial electron confinement would be by electrostatic reflection at the extraction plane, which is biased negatively with respect to the plasma potential, and, at the other end, would be by mirror action through adiabaticity of the magnetic moment. Radial confinement of the argon ions may be electrostatic since the electrons are well tied to the field lines. Thus, to the extent that cross field diffusion is not a dominant process the only loss of ions should occur at the small area of the throat region and at the screen grid.

4.3.2 Microwave Circuit

Microwave power for the experiment was supplied by a Varian VA888b klystron amplifier operating at 5 GHz at output power levels of up to 1 kW cw at the tube. The klystron amplifier electrical efficiency at full output power is 28 percent. The circuit diagram shown in Figure 4-7 indicates the microwave configuration used to supply power to the thruster as well as the power monitoring and tube protection circuitry. The circulator is connected to act as an isolator and thus protects the amplifier from receiving excessive and damaging reflected power from circuit impedance mismatches. Power was transmitted by fundamental mode c-band waveguide. The forward power coupling monitor was calibrated calorimetrically by placing a matched water cooled load where the guide enters the thruster chamber. A copper termination block was inserted in place of the matched load in order to calibrate the reflected power monitor; the measured reflected power, with the copper short in position, as a function of forward power is shown in Figure 4-8. Also shown in that figure is the amount of power reflected when the copper short was taken out and the thruster

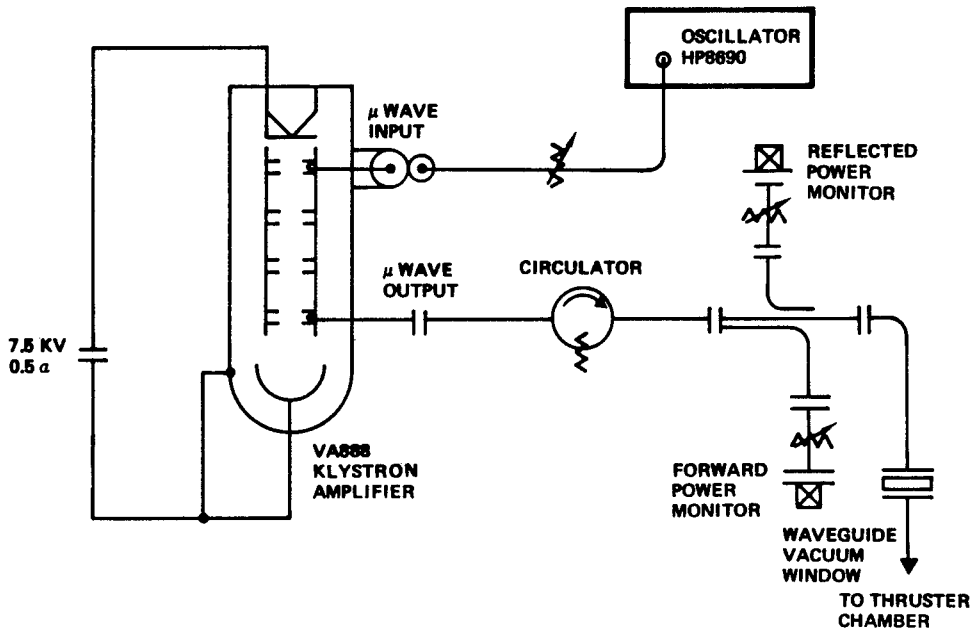

Figure 4-7. C-band microwave circuit for ECH source; 4.4 to 5 GHz, 1.4 kW CW

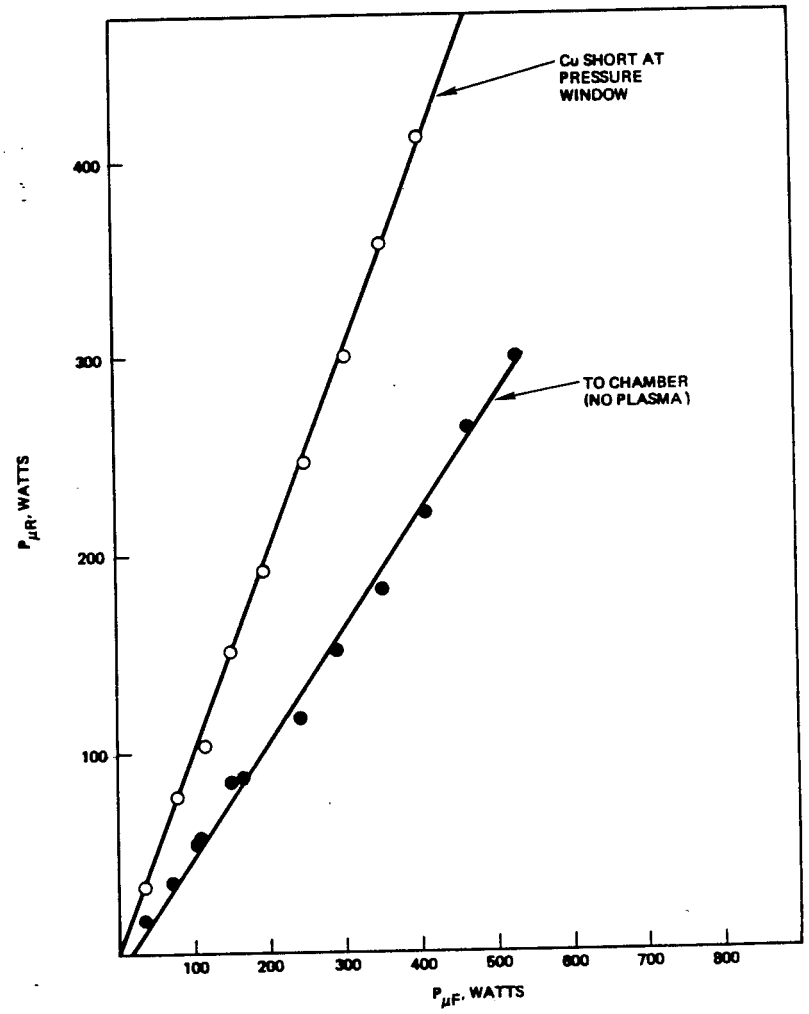

Figure 4-8. Measured reflected microwave power as a function of forward power with no plasma

chamber was connected to the guide. It appears that without plasma the high Q thruster chamber, which was constructed of welded aluminum and had no microwave absorptive materials in the interior, was still able to absorb or leak an appreciable fraction of the forward microwave power. We mention this because correct calibration of the forward and reflected power is of course important for an accurate determination of the eV/ion. We ascertain that the forward power calibration measurement is accurate to 10 percent but that the reflected power measurement may have a higher uncertainty.

4.3.3 Operation of Initial Configuration

The first test of the solenoidal-B field ECH plasma generator was made with the configuration as shown in Figure 4-6. The first pair of electromagnets was constructed of closely spaced solid conductor magnet wire and was water cooled only at their outer edges. Internal copper heat fins running radially from the center to the outer edges were to provide conduction of heat by ohmic losses from the central regions. The design specification was that the magnets were to operate up to a maximum series current of 180 amperes through the 96 turn windings of each magnet. The total voltage drop across the pair of pancakes connected in series was to be 25 volts. Upon testing these electromagnets it was found that their IR-drop was considerably higher than the manufacturer had quoted. In addition, the water cooling or heat exchange on the magnets was found to be insufficient. Nevertheless, with the acquisition of a new magnet power supply having higher voltage output, we were able to operate the magnets for short time periods, sufficient for some initial testing of this configuration. The measured on-axis magnet field strength produced by these electromagnets operating at 80 amperes is shown in Figure 4-9.

For initial operation, no microwave limiters were used near the mirror region. To ignite the plasma, the chamber pressure had to be raised to 5 mtorr but after the discharge was started could be lowered to an operating level of 5×10^{-4} torr. In this configuration the discharge, as viewed through the perforated copper extraction plate, appeared to be confined to only the small anti-chamber region surrounded by the electromagnets and very little ion current (100 ma) could be collected at the negatively biased extraction plane. This was surprising to us since we had thought that, even though the ECH heating zone was located in the mirror

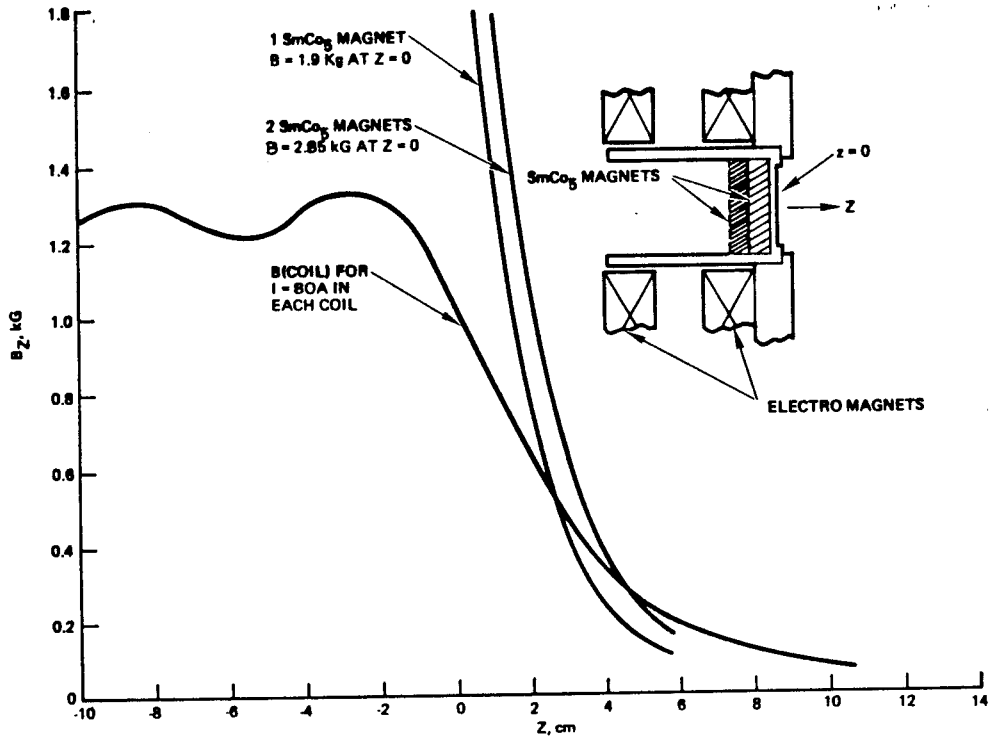

Figure 4-9. Placement location of the SmCo disks and resultant on-axis magnetic field strength

region of the anti-chamber, the heated electrons would find their way along the field lines out to the larger solenoid field volume and, thus, produce plasma in that region. It appears, however, that the electrons are lost rapidly to the walls resulting in rather poor performance with this configuration. In addition, the conversion efficiency was very poor with 70 to 80 percent of the forward power being reflected back down the power feed. We mention that the inner diameter of the anti-chamber was 4.4 cm, just large enough to propagate the TE_{11} cylindrical mode in a vacuum.

4.3.4 Revised Configuration

As a result of this initial performance it was decided to eliminate the anti-chamber region from the vacuum volume and to form a heating zone in the solenoidal part of the vacuum chamber. Since the electromagnets could not be operated at high enough currents to produce the ECH zone at sufficient distances from the chamber wall, two 5 cm diameter, 1.3 cm thick $SMCO_5$ disk magnets were placed at the position shown in Figure 4-9. Also indicated is the resulting on-axis axial magnetic field. The mod-B resonance surface for 5 GHz of 1.7K g is now placed about 1.0 cm from the wall even when the electromagnet current is zero. In addition, it should be noted that the field line divergence with these permanent magnets is somewhat greater than indicated in Figure 4-6 for the electromagnets. Discharge operation with the combination of two rare-earth permanent magnets and the electromagnets, now butted together, was considerably improved. We were able to collect up to 2 amperes of ion current at the extraction plane with an energy expenditure of about 200 watts per ampere. However, because of the severe over-heating problem with the electromagnets, detailed probing and measurement could not be carried out.

A new pair of electromagnets having the same outer dimensions as the original set were therefore designed and procured. Each new pancake had turns of hollow core copper, 0.188-inch square, and with proper water coolant could be operated continuously at currents of up to 500 amperes. The ampere-turns and magnetic field distribution inside the thruster using this second pair of magnets was very similar to that produced with the first 96-turn pancakes. The measured axial magnetic field at z = 0 (see insert Figure 4-9 for coordinate identification) as a function of the series current is shown in Figure 4-10a and the axial variation of B_z is

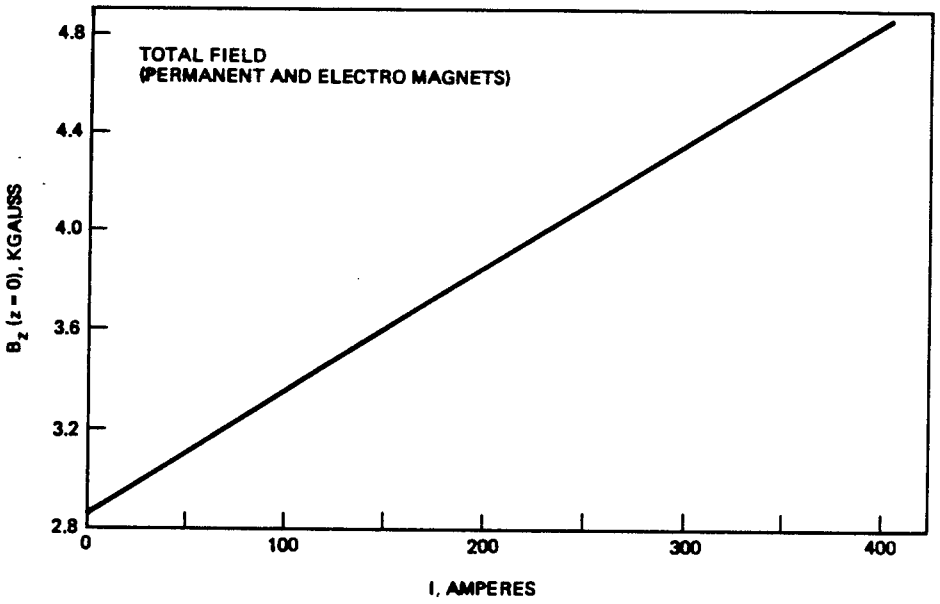

Figure 4-10a. Variation of B_z at Z = 0 as a function of the series current in the improved electromagnets.

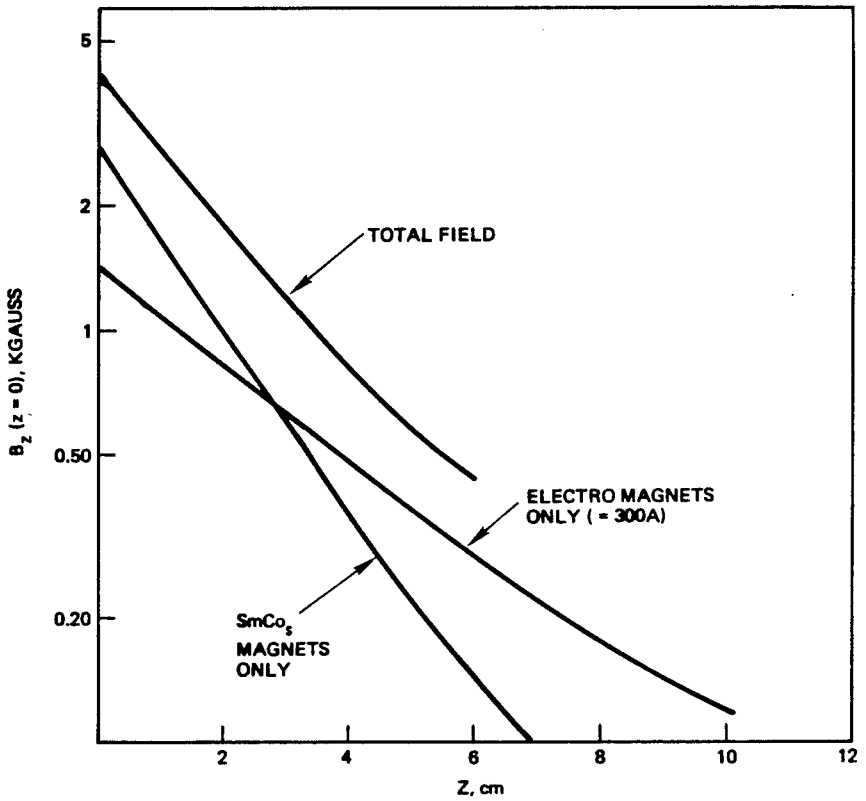

Figure 4-10b. Axial variation of the on-axis B_z for the improved electromagnets

indicated in Figure 4-10b. Note that the resonant surface, B = 1.7K g, is a little more than 2 cm away from the inner vacuum wall when the magnet current is 300 A; considering the representative magnetic field plot of Figure 4-6 this means that, without a microwave limiter, plasma should be produced on almost all field lines in the thruster; hence, the energy expenditure, which is not expected to be very good without limiters, should improve when the limiters are in place.

The final solenoidal configuration which was used, and from which the data presented in the remainder of this section was obtained, is shown in Figure 4-11. Two Samarium-Cobalt magnet disks are situated in the center of the thruster backplate and are surrounded by the two new electromagnets butted against each other. Superposed on the plasma volume in that figure is an iron-filing map of the field lines produced by the electromagnets only. The microwave power feed location remained unchanged from that shown in Figure 4-6. The extraction plane, which was a perforated copper plate, simulated, as in previous experiments, beam extraction when biased with respect to the thruster radial walls and backplate. Ion current collection probes, P1-P6, were mounted flush to the radial walls. Also indicated in Figure 4-11 is the location of the limiter when it was used and the gas feed.

4.3.5 Test Results Without Limiter

The operating parameters of this configuration, without a limiter, are given in Table 4-1. Indicated is the quantity of argon ion current (I_g) collected at the extraction plane as a function of the extraction plane grid bias (V_G) and electromagnet current (I_m) for a constant forward microwave power (P_F) of 600 watts. For a constant magnet current, the ion current to the grid is seen to increase as the grid bias becomes more negative. This would seem to indicate electrostatic reflection of electrons by the extraction plane as originally hypothesized. However, the electron temperature as measured by a Langmuir probe was only 6 eV to 8 eV and the plasma potential with respect to the radial walls was 16 to 20. eV. Thus, it is difficult to see how a 35 volt increase in grid bias would cause a considerable (30 percent) increase in grid current when the bulk of electrons, which presumably have a Maxwellian distribution, are already reflected by the plasma sheath near the grid when it is biased at -50 volts. The increase in grid

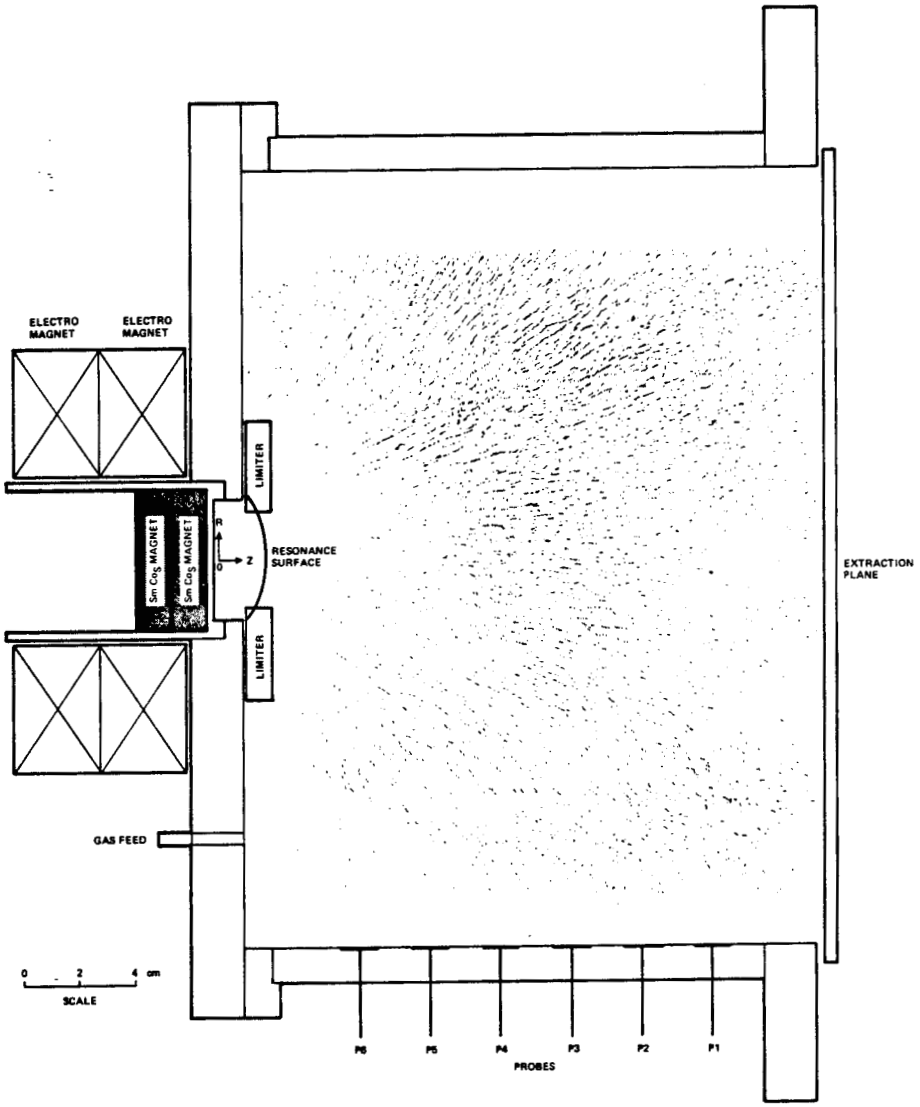

Figure 4-11. Final solenoidal configuration tested

Table 4-1. Solenoidal B-field plasma generator operating parameters (no limiter)

I_M(A)	V_G(V)	I_G(A)	$P_{\mu F}$(W)	$P_{\mu R}$(W)	eV/ION	I_{P1}(mA)	I_{P2}(mA)	I_{P3}(mA)	I_{P4}(mA)	I_{P5}(mA)
300.	-50.	1.5	600.	140.	310.	2.35	1.8	1.25	0.87	0.45
300.	-65.	1.75	600.	140.	260.	2.35	1.75	1.20	0.88	0.49
300.	-75.	1.85	600.	110.	260.	2.55	2.2	1.40	0.92	0.45
300.	-85.	2.00	600.	80.	260.	2.65	2.4	1.50	0.94	0.40
200	-50.	1.3	600.	300.	240.	--	---	--	--	--
150.	-50.	0.78	600.	430.	220.	--	---	--	--	--
100.	-50.	0.45	600.	510.	220.	0.75	1.0	0.62	0.45	0.26
0.0	-50.	0.35	600.	510.	260.	0.65	1.0	0.72	0.65	0.51

$P_0 = 5.5 \times 10^{-4}$ Torr, Argon

Probe Bias (p1 - p5) at -40.V

current with increasing negative grid bias may be due to secondary electron emission from the grid but operation of this thruster with various gasses (krypton and xenon) as described below does not indicate that this is the case. Note also that the amount of reflected microwave power decreases with increasing negative grid bias in just such a way as to keep the eV/ion value essentially constant. The mechanism for this is not easily understood.

At a constant grid bias the current collected by the grid was reduced substantially as the magnet current was lowered but the eV/ion value did not change dramatically as is indicated in Table 4-1. This would be expected if the fraction of ions lost to the radial walls and to the backplate is not a strong fuction of the magnetic field amplitude as would be the case since, without a limiter, a substantial portion of the plasma-filled magnetic field lines do not terminate at the extraction plane. The increase in the reflected microwave power as the magnet current is reduced may simply mean an increase in plasma density on those field lines which terminate at or near the microwave power feed. A suitably placed limiter should thus reduce the reflected power level.

Further evidence of considerable ion loss to non-extraction surfaces is indicated in Table 4-1 by the amout of ion current, I_{p1} through I_{p5}, collected by the wall probes, P1 through P5, which were biased at -40 volts. Each of these probes had a collection area of 1.27 cm^2. It is seen that the ion current density to the cylindrical walls of the thruster gradually decreases in the upstream direction toward the backplate. Note that the current density to these probes is little affected as the grid current is varied by changing the grid bias. This indicates that variation of the grid bias does not influence cross-field transport nor does it substantially change the microwave field structure within the thruster cavity. However, the current density to these probes is changed when the pancake magnet current is reduced; in comparing the grid current with the current to each of these probes it appears that proportionately more current is lost to the radial walls as the magnet current is reduced. One would expect this since the magnet field, which is the sum of fields from both the permanent and electromagnets, becomes more divergent as the electromagnet current is reduced. Again, it is not clear why empirically the eV/ion value remains essentially unchanged.

Probes similar to those mounted on the cylindrical wall were also placed on the extraction grid to obtain a measure of the radial plasma uniformity, which ultimately would be translated to the beam flatness. The result of these measurements is shown in Figure 4-12. Plasma uniformity is not very good but this was expected since flux tubes at outer radial positions expand to larger areas at the extraction plane than those flux tubes nearer the center (r = 0) of the device.

To ascertain whether or not plasma is channeled along the magnetic field lines between the backplate and the extraction plane, we constructed a Langmuir probe (0.023 cm diameter, 0.40 cm long tungsten tip) which was inserted at probe position P6 in Figure 4-11 and which could be moved radially in and out. The result of the radial density and electron temperature variation measured with this probe is indicated in Figure 4-13. It is seen that the electron density varies by a factor of 10 as the probe is moved from a radial position of r ≃ 5 cm to the center of the device. There is thus a rather steep radial density gradient nearest the high field regions of the device as had been anticipated when this solenoidal concept was originated. The measured electron temperature is seen to take a discontinuous jump at r ≃ 1 to 2 cm which may be due to non-uniform illumination of the heating zone by the microwave fields, assuming that the probe has a non-perturbing effect.

It is interesting to compare the measured plasma density at z = 5.2 cm shown in Figure 4-13 with the current density shown in Figure 4-12 at the extraction plane. The maximum plasma density at z = 5.2 cm was about 2.0 x $10^{11}/cm^{-3}$ which is very close to the microwave cutoff density given by $\omega_{pe} = \omega_{\mu}$ for 5 GHz power. The maximum current density at the extraction plane was about 7 mA/cm^2 and also occured at the radial center, r ≃ o. If we assume an electron temperature at the extraction plane of 3.5 eV and use the formula for a stable sheath

$$J \simeq 0.5\ nec_s$$

where J is the current density, n the plasma density and c_s the sound speed we obtain a current density of J ≃ 7 mA/cm^2 for n ≃ 3 x $10^{11}/cm^3$. This means that, at least near r ≃ o, the plasma density is axially nearly uniform and does not increase in the direction of higher magetic field strength! This comparison also indicates that the maximum extraction

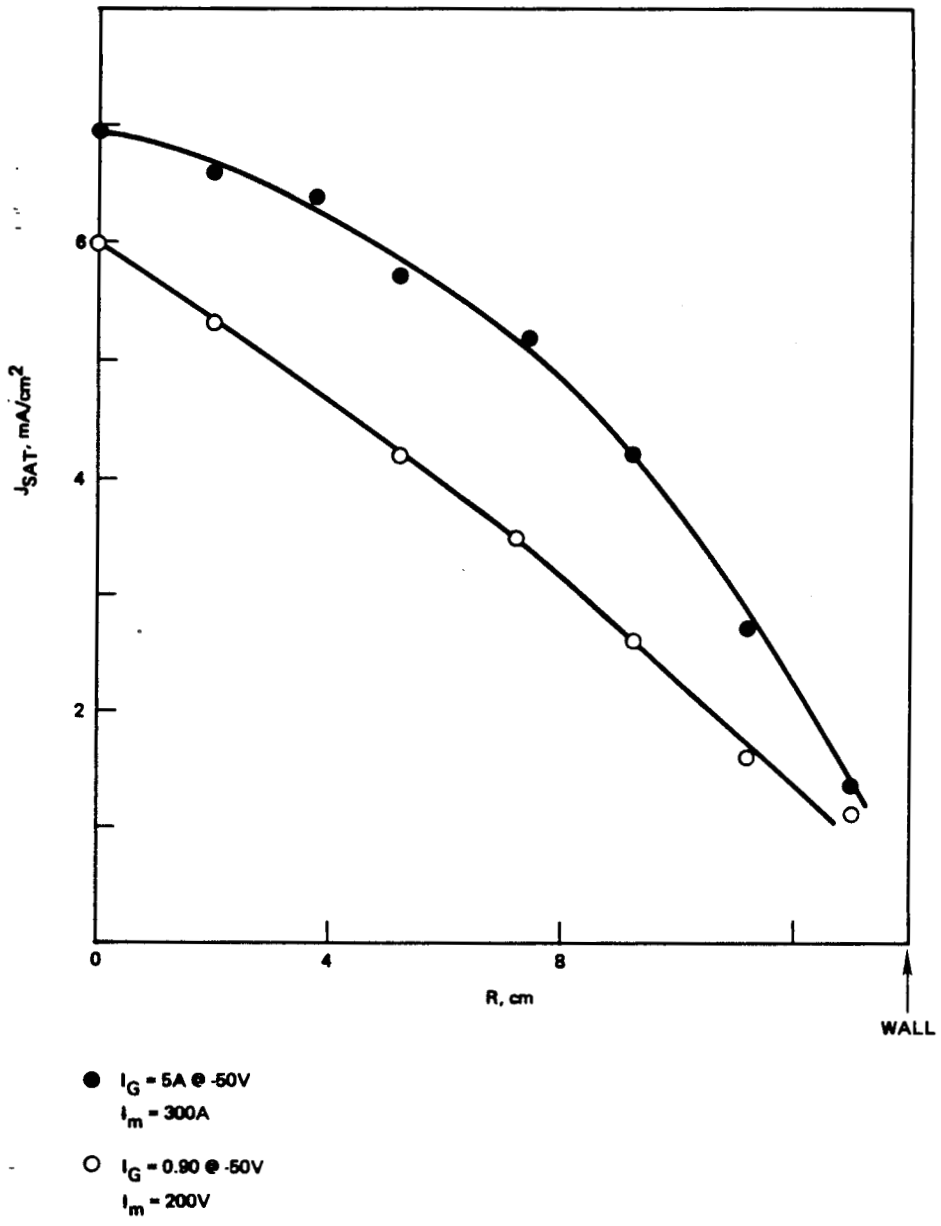

Figure 4-12. Radial ion saturation current profile at the extraction plane

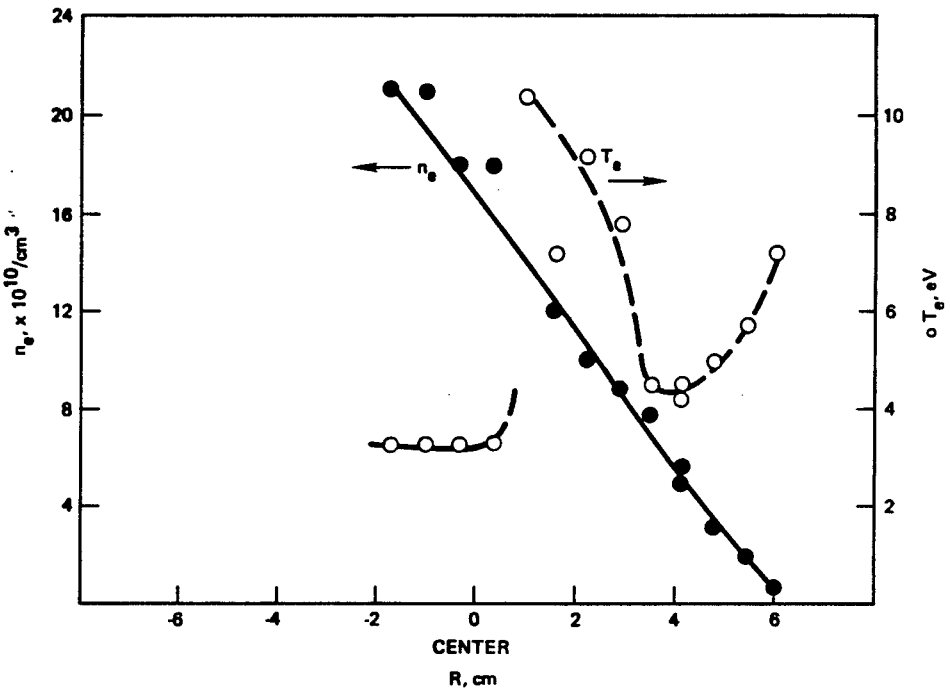

Figure 4-13. Radial electron temperature and density measure with a Langmuir probe inserted at probe position P6.

current (about 2 amperes) which we were able to collect on the 28 cm diameter extraction grid is limited by the microwave cutoff condition $\omega_{pe} = \omega_{\mu}$ as was the case with the axial and azimuthal permanent magnet devices discussed earlier in Section 4.2.

4.3.6 Evidence of Density Saturation

Further evidence that the maximum ion current collected by the extraction plane was limited by microwave cutoff is given in Table 4-2. Shown in this table are the measured grid currents for various grid bias conditions for operation with three different gasses: argon, krypton and xenon. Operation with each of these gases was with a constant forward microwave power level of 700 watts. As for argon, the grid current increased with increasing negative grid bias for both kryption and xenon, although the magnitude of the grid current, at a given bias level, decreases as the ion mass goes up. This latter fact is expected if the grid current obeys the functional relation $I_G \propto (T_e/M_{ION})^{1/2}$. In fact, above about -40 volt grid bias, the ratio of grid currents I(argon)/I(krypton) and I(argon)/I(xenon) becomes constant and equal to the inverse ratio of the square root of the ion masses. That is,

$$I(\text{argon})/I(\text{kryption}) = \left(M(\text{krypton})/M(\text{argon})\right)^{1/2} = 1.45$$

and

$$I(\text{argon})/I(\text{xenon}) = \left(M(\text{xenon})/M(\text{argon})\right)^{1/2} = 1.8$$

This would not be the case if the plasma density, whatever its distribution at the extraction plane may be, had not reached its maximum value. Further, this maximum density cannot depend on the type of gas since the ionization and excitation rates vary considerably for argon, krypton, and xenon. Therefore, the maximum density, and hence the maximum grid current at a given bias, must be determined by the microwave frequency used. With a forward power of 700 watts we always measured a considerable amount of reflected power so the density was not power limited. Of course, the ev/ion, which is obtained from the net microwave power divided by the grid current, decreased successively in going from argon to krypton to xenon since the ionizatin cross-sections by electron impact increase successively in the same order.

Table 4-2. Extraction current comparison for operation with Argon, Krypton, and Xenon

V_G(V)	Argon I_G(A)	Krypton I_G(A)	Xenon I_G(A)	I_A/I_{Kr}	I_A/I_{Xe}
-20.	0.2	0.20	0.28	1.0	0.71
-30.	0.8	0.55	0.58	1.45	1.34
-40.	1.2	0.80	0.72	1.5	1.67
-50.	1.5	0.95	0.82	1.58	1.83
-60.	1.65	1.05	0.91	1.57	1.81
-70.	1.8	1.20	0.99	1.50	1.82
-80.	1.95	1.35	1.05	1.44	1.86
-90.	2.1	1.40	1.10	1.50	1.91

$P_{\mu F}$ = 700. watt

I_m = 300. Amp.

Table 4.2 Extraction current comparison for operation with Argon, Krypton, and Xenon

4.3.7 Test Results with Limiter

Operation of the solenoidal B-field thruster without a limiter yielded an efficiency of 260 eV/ion as indicated in Table 4-1. Operation with a suitably chosen limiter which prevents electron heating and plasma production on those field lines which intercept the radial wall should improve the performance. The iron-filing map in Figure 4-11 and the computer generated field plot in Figure 4-6 were used as a guide in choosing the limiter dimensions which would eliminate the resonant surfaces for fundamental heating on those field lines which go to the radial walls. The limiter dimensions chosen were an annulus of thickness 1.0 cm, inner diameter of 3.3 cm and outer diameter of 8.0 cm. This annulus was mounted to the backplate as shown in Figure 4-11.

Some results of operation with this limiter are given in Table 4-3. Quite unexpectedly, the eV/ion values were considerably higher with the limiter in place than in operation without a limiter. One might speculate that the limiter dimensions were chosen incorrectly so that plasma is channeled to a small central portion of the extraction plane. If it were the case that the effective extraction area has been reduced by the limiter then the eV/ion, which is calculated from P_μ/I_G, would increase simply because less total grid current is available. However, this argument cannot be correct since we have already demonstrated that a maximum density has been reached and that presumably the net microwave power goes only to feed energy to the plasma channel. Thus, if anything, the ev/ion should have decreased since it has been demonstrated in Figure 4-12 that the density peaks in the radial center. A radial ion current density profile at the extraction plane was unfortunately not taken. The reasons for the less efficient operation with the limiter has not been resolved.

At this point of the experimentation with the microwave solenoidal B-field thruster was terminated in order to divert more resources to the more promising RFI thruster development already discussed earlier in this report.

4.4 SUMMARY AND DISCUSSION

We have presented some of the operational characteristics of a 30 cm thruster which utilizes a solenoidal or mildly divergent volume magnetic field geometry for plasma confinement and electron cyclotron resonance

Table 4-3. Solenoidal B-field plasma generator operating parameters (with limiter)

I_M(A)	I_G(A)	$P_{\mu F}$(W)	$P_{\mu R}$(W)	eV/ION
300.	1.55	700.	160.	348.
250.	1.40	700.	180.	371.
200.	1.30	700.	210.	377.
150.	1.20	700.	233.	389.
100.	1.18	700.	304.	335.
50.	0.85	700.	320.	445.
0.0	0.30	700.	551.	497.

$P_0 = 6. \times 10^{-4}$, ARGON

GRID BIAS AT -50.V

heating with microwaves at a frequency 5 GHz for plasma production. The volume magnetic field was produced by a combination of permanent magnets and variable-field magnets. We have succeeded in producing a steady plasma in this configuration whose density is limited by the microwave frequency used.

The original propose in building and testing a thruster with this magnetic field configuration was to study cross-field plasma transport. We specifically wanted to test the degree to which plasma could be channeled along magnetic field lines which are intercepted by the thruster ion extraction plane even though the strength of the magnetic field near the extraction grid was such that ions, but not electrons, could be considered unmagnetized. It was anticipated that a study of this solenoidal magnetic geometry would aid in identifying a configuration which utilized only permanet magnets and yielded a more energy efficient thruster than had been previously developed under the initial phase of this program.

The degree to which we have succeeded in our original purpose is clear. In all probablility the axial losses of both ions and electrons exceeded the radial losses. Although we have demonstrated that the ion extraction current is dependent on the value of the negative grid bias potential, the fact is that the eV/ion does not vary substantially. Furthermore, the eV/ion did not change drastically when the magnetic field strength from the electromagnets was reduced. Finally, and most perplexing, was the demonstration that the eV/ion increased considerably when a limiter, which was to channel the plasma to the grid and reduce radial wall losses, was introduced.

Although the results of the solenoidal configuration described here are not very positive, one should nevertheless not overlook the possible applications of a plasma generator concept based on electron cyclotron heating. The ECH plasma generator with permanent magnets arranged in an azimuthal cusp geometry which was developed and described under the first phase of this program performed very well in terms of electrical efficiency, reliability, and simplicity of operation. It provided a steady state, uniform plasma density of $3 \times 10^{11}/cm^3$, limited by the frequency of the microwaves. Most importantly, as with all the ECH plasma generator configurations we have tested, this device contained no internal electrode structure or antenna and could thus produce plasmas of exotic materials (be

they insulators, metals or corrosives) which would be very difficult to produce with a hollow cathode, arc, filament, or RFI discharge. We have serious reservations that the type of ECH plasma generator discussed in this report could complete with a hollow cathode or RFI discharge for electrostatic thruster application should it ever arise.

5. REFERENCES

Section 2

1. W. D. Ramsey, J. Spacecraft Rockets 9, 318 (1972).

2. R. Limpaecher and K. Mackenzie, Rev. Sci. Instr. 44, 726 (1973).

3. W. L. Stirling, P. N. Ryan, C. C. Tsai and K. N. Leung, "Magnetic Multipole Line-Cusp Plasma Generator for Neutral Beam Injectors," Rev. Sci. Instr. 50, 102 (1979).

4. W. F. DiVergilio, H. Goede, V. V. Fosnight, "High Frequency Plasma Generators for Ion Thrusters," Interim Report NASA Cr-167957, Nov. 1981.

Section 3

1. W. Hittorf, Ann Physik 21, 137 (1984).

2. G. Francis, "Ionization Phenomena in Gases," Academic, New York (1960).

3. R. J. Sovie and G. R. Seikel, "Radio-Frequency Induction Heating of Low-Pressure Plasmas," NASA Technical Note NASA TND-4206 (1967).

4. H. W. Loeb, "Recent Work on Radio Frequency Ion Thrusters," AIAA Paper No. 70-1102 (1970).

5. T. K. Samec, "Plasma Confinement by Surface Magnetic Fields," UCLA Plasma Physics Group Report PPG-281, (November 1976).

6. Goede, J. M. Dawson, K. R. MacKenzie, "Observation of Anomalous Penetration of RF Fields in a Collisionless Plasma," Phys. Rev. Lett. 44, 1066 (1980).

Section 4

1. R. A. Dandl, A. C. England, W. B. and H. O. Eason, M. C. Becker and G. M. Haas, Nuclear Fusion 4, 344 (1964).

2. J. C. Sprott, Phys. Fl. 14, 1975 (1971).

3. D. B. Miller and E. F. Gibbons, "Cyclotron Resonance Propulsion System," NASA Contractor Report, Vo. Cr-42336, 1963.

4. W. F. DiVergilio, H. Goede, V. V. Fosnight, "High Frequency Plasma Generators for Ion Thrusters," Interim Report NASA Cr-167957, Nov. 1981.

5. Field calculations shown in Figure 4-6 were computer generated by Dr. B. Hauss.